Hydrogen loop configurations for PEM fuel cells

Master Thesis

Jasper Ros

TU Delft

Hydrogen loop configurations for PEM fuel cells

Master Thesis

by

Jasper Ros

to obtain the degree of Master of Science
in Offshore & Dredging Engineering with the specialization of Offshore Renewable Energy
at the Delft University of Technology,
to be defended publicly on Wednesday June 18, 2025 at 10:00 AM.

Student number:	4715845	
Project duration:	September 1, 2024 – May 31, 2025	
Thesis committee:	Dr. ir. L. van Biert,	TU Delft, supervisor
	Dr. ir. P. de Vos,	TU Delft
	Ir. D. de Jong,	Future Proof Shipping

Cover: The H2 Barge 1 owned by Future Proof Shipping [1]

An electronic version of this thesis is available at http://repository.tudelft.nl/.

TU Delft FPS

Preface & Acknowledgements

This thesis marks the end of my master's in Offshore and Dredging Engineering and wraps up a longer chapter of studying Mechanical Engineering. Over the past few years, I have had the chance to dive into a range of engineering topics, but it was not until I took a gap year to join Forze Hydrogen Racing that I really got hooked on hydrogen and fuel cell technology. That year turned out to be a turning point, it gave me hands-on experience with the challenges of hydrogen systems and sparked the curiosity that eventually led to this thesis.

That curiosity turned into a full research project thanks to Future Proof Shipping. After seeing a schematic of the Balance of Plant on one of their hydrogen-powered vessels, I was struck by how different it looked from what I had worked on at Forze. That simple observation set everything in motion. I wanted to understand why those design choices were made and what trade-offs they involved. That became the basis for this thesis, building a dynamic MATLAB Simulink model to simulate and compare hydrogen loop configurations under realistic maritime conditions

I would like to acknowledge the use of AI tools in writing this report. These tools were used exclusively to refine phrasing and enhance the clarity of the text. All of the technical work, modeling, analysis, and conclusions are my own and were developed using standard engineering methods. Everything you see here is based on physics, simulation results, and real-world validation.

I would like to thank Lindert van Biert for his support, guidance, constructive feedback, and encouragement throughout the process. Our weekly meetings were a great space to work through both the technical and structural parts of this project. I'm also very grateful to Milinko Godjevac, who gave me the opportunity to do my thesis at Future Proof Shipping and for encouraging me to think critically and challenge assumptions. After Milinko's departure, Dirk de Jong kindly took over and offered valuable support throughout the remainder of the project. A special thanks goes to the entire team at Future Proof Shipping for sharing their time, expertise, and their ship's data. Their openness made it possible to validate the model and ground the research in real-world applications.

Finally, I would like to thank the people in my personal life, especially my parents and my girlfriend, for their constant support, encouragement, and patience throughout this journey.

Jasper Ros
Delft, May 2025

Abstract

The transition to sustainable propulsion in maritime transport has highlighted hydrogen-fueled PEM fuel cells as a compelling alternative to conventional diesel engines, driven by increasingly stringent emission regulations. While significant research has focused on single fuel cells or complete stacks, the hydrogen loop, the subsystem responsible for delivering, recirculating hydrogen, remains underexplored, particularly in the context of maritime applications. The hydrogen loop plays a critical role in determining system efficiency, reliability, and performance. Improper management of flow, pressure, temperature, and humidity can lead to lower efficiency, membrane dehydration, flooding, or even irreversible damage to the stack. To address this, a novel dynamic MATLAB Simulink model was developed to evaluate hydrogen loop configurations under realistic maritime conditions.

This thesis investigates the design and performance of twelve distinct hydrogen loop configurations, each comprising different combinations of supply and recirculation components such as pressure regulators, proportional valves, mass flow controllers, liquid ring pumps, blowers, and ejectors. The configurations are motivated by real-world implementations from an inland vessel and a fuel cell-powered race car, as well as conceptual arrangements aimed at exploring broader designs. A novel, dynamic MATLAB Simulink model was developed that uniquely integrates pressure, temperature, humidity, two-phase flow, and phase change dynamics, to capture both transient and steady-state behavior of hydrogen loops under realistic maritime conditions. Unlike existing models, it allows detailed component-level interaction analysis and configuration-specific scoring under a standardized testing framework. Key governing equations are based on established physics principles, and the model is validated using experimental data from the H2 Barge 1, an operational hydrogen-powered inland vessel from Future Proof Shipping.

Each configuration is evaluated across a range of criteria, including hydrogen utilization, power consumption, performance, pressure and temperature robustness, stoichiometry control, and system response under transient loads. Special attention is given to component interactions that influence overall system behavior, such as the influence a recirculation device has on humidity and temperature, or the limitations of ejectors in low-load scenarios due to their dependency on primary flow pressure. Hybrid configurations combining ejectors with mechanical pumps are also explored to mitigate operational limitations at low power setpoints.

The results highlight that hydrogen loop configuration choices have a significant impact on system performance, control flexibility, and design complexity. Ejector-based systems are energy-efficient and mechanically simple but suffer from limited operational range and lack dynamic control, especially at low loads. Mechanical recirculation devices like blowers and liquid ring pumps offer robust performance across the full load range and enable flexible operation, though they come with higher energy consumption and potential mechanical wear. Supply components also influence system behavior: proportional valves allow dynamic pressure control but require careful tuning, while mass flow controllers simplify control logic but lack pressure regulation. Hybrid solutions, combining ejectors with pumps, can mitigate some limitations but add complexity. Among the twelve configurations studied, the proportional valve–blower setup emerges as the most suitable for maritime fuel cell applications, offering the best balance of efficiency, operational flexibility, robustness, and system simplicity.

Ultimately, this research provides a structured methodology for comparing hydrogen loop configurations, enabling system designers to make informed decisions based on specific performance requirements and operational constraints. The findings underscore the importance of integrated system modeling in BoP design and contribute to the broader goal of developing scalable, reliable, and efficient hydrogen propulsion systems for maritime applications.

Contents

Nomenclature

Abbreviations

Abbreviation	Definition
BoP	Balance of Plant
FC	Fuel Cell
GDL	Gas Diffusion Layer
HRB	Hydrogen Recirculation Blower
LRP	Liquid Ring Pump
MFC	Mass Flow Controller
PEM	Proton Exchange Membrane
PID	Proportional-Integral-Derivative
PR	Pressure Regulator
PRV	Pressure Relief valve
PV	Proportional Valve
P&ID	Piping and Instrumentation Diagram
RPM	Rotations Per Minute

Symbols

Symbol	Definition	Unit
A	Area	[m^2]
C	Chisholm constant	[-]
C_i	Volumetric concentration	[%]
Cp	Specific heat capacity	[J/kg*K]
D	Diameter	[m]
D_v	Diffusion coefficient	[m^2/s]
F	Faraday constant	[96485 C/mol]
f	Friction factor	[kJ/kg]
g	Gravitational constant	[m/s^2]
Gr	Grashof number	[-]
H	Enthalpy of vaporization	[kJ/kg]
h_m	Mass transfer coefficient	[m/s]
h	Heat transfer coefficient	[W/m^2K]
I	Current	[A]
J	Current density	[A/cm^2]
Kv	Flow factor	[m^3/h]
K	Thermal conductivity	[W/mK]
L	Length	[m]
M	Molar mass	[g/mol]
M	mass	[kg]
$\dot{m}$	Mass flow	[g/s]
n	number of moles	[-]
Nu	Nusselt number	[-]
P	Power	[kW]
Pr	Prandtl number	[-]
p	Pressure	[bar] or [mbar]

Symbol	Definition	Unit
Q	Heat	[J]
$\dot{Q}$	Heat flow	[J/s]
Re	Reynolds number	[-]
RH	Relative humidity	[%]
R	Gas constant	[8.314 J/K*mol]
R	Thermal resistance	[K/w]
Ra	Rayleigh number	[-]
Sh	Sherwood number	[-]
Sc	Schmidt number	[-]
T	Temperature	[°C] or [K]
U	Heat transfer coefficient	[W/m^{2}K]
v	Velocity	[m/s]
$\dot{V}$	Volume flow rate	[m^3/s]
x	Molar concentration	[%]
β	Coefficient of volume expansion	[1/T]
ε	Pipe roughness	[m]
μ	Dynamic viscosity	[Pa*s]
ν	Kinematic viscosity	[m^2/s]
ρ	Density	[kg/m^3]
ϕ	Interaction parameter	[-]
Φ	Two-phase multiplier	[-]
χ	Lockhart-Martinelli parameter	[-]
ω	Entrainment ratio	[-]

1 Introduction

As the maritime sector seeks to reduce emissions and meet increasingly stringent environmental regulations, hydrogen-fueled proton exchange membrane (PEM) fuel cells have emerged as a promising alternative to conventional diesel propulsion. PEM fuel cells emit only water, unlike combustion-based systems, making them especially attractive for environmentally sensitive applications such as inland and coastal shipping. A major challenge in applying PEM fuel cells to maritime systems lies in engineering a robust and efficient hydrogen supply and recirculation system, often referred to as the hydrogen loop.

While the fuel cell stack itself has been widely studied, both experimentally and numerically, far less attention has been given to the Balance of Plant (BoP), the support systems responsible for fuel and air supply, heat and water management, and power conditioning. Within the BoP, the hydrogen loop plays a key role in determining overall system efficiency, performance, reliability, and lifetime. Properly managing hydrogen delivery and recirculation is essential not only for optimizing stack performance but also for preventing issues such as membrane dehydration, flooding, and performance degradation due to nitrogen accumulation.

The hydrogen loop is a complex system involving a variety of active and passive components, including supply valves, recirculation pumps, water separators, purge valves, pressure relief valves and sensors. Each component impacts key operating parameters such as pressure, temperature, humidity, and hydrogen stoichiometry. Despite its importance, a systematic comparison of different hydrogen loop configurations under dynamic maritime operating conditions remains lacking.

Existing research has often focused on isolated aspects of the BoP. Comparative studies on mechanical pumps, ejectors, and electrochemical pumps have primarily evaluated power consumption, with ejectors generally showing the lowest power use, followed by electrochemical and mechanical pumps [2]. Conceptual comparisons of hydrogen supply configurations exist [3], but many lack empirical data or simulations. Studies have shown that recirculation improves fuel efficiency compared to dead-end anodes, with optimal purging strategies enhancing performance [4, 5]. For instance, a 2 kW and a 6.5 kW system both demonstrated improved efficiency with periodic purging.

Research into similar Nedstack fuel cells, such as those examined in this study, revealed performance sensitivity to pressure fluctuations during purging [6]. At the component level, numerous investigations have examined specific BoP elements, including scroll compressors [7], regenerative blowers [8], pressure regulators [9, 10], and liquid ring pumps [11]. Modeling assumptions for isothermal liquid ring pump operation have also been established [12]. Additionally, stack-level studies have highlighted the impact of operating temperature, pressure, and membrane properties on fuel cell voltage and efficiency [13, 14, 15].

Despite these efforts, thorough evaluations of complete hydrogen loop designs, especially those tailored to maritime fuel cell applications, are rare. Comparative studies have largely targeted automotive

or stationary contexts, where system constraints and operational profiles will differ. This research addresses that gap by presenting a comprehensive modeling and simulation study of twelve distinct hydrogen loop configurations, combining various supply and recirculation devices. Using a MATLAB Simulink-based model that incorporates key physical processes such as pressure, humidity, flow, and heat transfer, the study evaluates each configuration across multiple performance criteria. These performance criteria include efficiency, robustness to temperature and pressure changes, and hydrogen utilization.

The key research question is: *What are the most suitable hydrogen loop configurations for maritime applications?*

By integrating engineering analysis with realistic maritime performance demands, this work aims to provide practical insights into the optimal design of hydrogen loops for fuel cell BoPs. The findings contribute to a more complete understanding of the trade-offs between system complexity, control flexibility, and operational reliability, helping pave the way toward scalable, robust, and efficient hydrogen-powered vessels.

2

PEM Fuel Cell Applications and Hydrogen Loop Design

PEM fuel cells are used in diverse applications, each with distinct requirements for system design and operation. This chapter provides the background needed to understand how hydrogen loop configurations are shaped for each application, particularly contrasting automotive and maritime fuel cell systems.

The chapter also introduces key hydrogen loop components such as supply, recirculation, and auxiliary devices, and explains their roles within the Balance of Plant. Two real-world configurations, one from an inland vessel and another from a hydrogen race car, are used to illustrate how these components can be arranged differently. These examples set the stage for the analysis of twelve configurations evaluated in later chapters.

2.1. BoP design

Proton exchange membrane fuel cells are highly versatile, offering a broad range of applications due to their high efficiency, rapid start-up time, and low operating temperature. Their primary applications can be categorized into stationary and transportation uses. Stationary applications include generators, backup power systems, and grid power support. Transportation applications encompass vehicles such as cars, buses, trucks, trains, and ships.

In a fuel cell system, the Balance of Plant refers to all components and subsystems necessary to support the operation of the fuel cell stack but excludes the stack itself. These components handle fuel delivery, air supply, heat management, water management, and power conditioning. This paper focuses exclusively on the hydrogen loop, which involves hydrogen supply and recirculation. While some fuel systems do not incorporate recirculation, these are excluded from consideration here, as the absence of recirculation significantly reduces fuel efficiency. The function of the hydrogen loop is to deliver hydrogen to the fuel cell at the correct critical parameters, such as pressure, mass flow, humidity, and temperature [3]. Proper control of these factors ensures optimal performance and efficiency. Failure to maintain these conditions can significantly reduce performance and, in severe cases, damage the stack.

Not all the hydrogen entering the stack is consumed during the electrochemical reaction. This is intentional, as supplying excess hydrogen helps prevent fuel starvation and associated efficiency losses. To improve overall fuel efficiency, the unused hydrogen is recirculated. This is achieved by maintaining a sufficiently high stoichiometry, defined as the ratio of hydrogen supplied to hydrogen actually consumed, as shown in equation 2.1.

$$\text{Stoichiometry} = \frac{\text{Hydrogen supplied}}{\text{Hydrogen consumed}} \tag{2.1}$$

In addition to improving fuel utilization, the recirculation loop also ensures that the hydrogen flow rate is high enough to remove excess liquid water from the anode side of the fuel cell. This is critical to prevent flooding, which can reduce performance or even damage the stack. A water separator is typically included in the loop to remove this liquid water, which is then discharged via a drain valve.

An added advantage of recirculation is its self-humidification effect. The hydrogen exiting the anode contains unreacted hydrogen and water, which mix with the incoming supply hydrogen to humidify the stream. Increased humidity enhances cell voltage, leading to improved efficiency and power output. Additionally, the counterflow configuration within the stack allows the cathode to further humidify the anode through the membrane [16]. For these reasons, dedicated humidifiers in the hydrogen loop are less common and have been omitted from this analysis.

2.2. Maritime compared to automotive applications

To effectively compare the configurations, it is essential to understand the key differences in their design objectives and operational criteria. These differences arise primarily from the distinct requirements and priorities in maritime and automotive applications.

2.2.1. Differences in BoP design

Balance of Plant (BoP) design in maritime and automotive fuel cell systems is driven by fundamentally different operational requirements and constraints. In maritime applications, large hydrogen storage volumes are required to meet extended range and power demands. As a result, system efficiency becomes a critical design goal. Since ships are not as limited by weight and volume as vehicles, power density can be sacrificed in favor of more efficient, lower-current-density operation. This design flexibility allows for BoPs that prioritize reliability, efficiency, and modularity over compactness. Modularity is a key advantage in maritime systems: containerized BoP units enable easier installation, scalability, and maintenance. Maritime BoPs are typically designed for power outputs exceeding 1 MW, and must operate continuously for long durations. To support this, long-term reliability is essential. One way this is achieved is through redundancy, equipping vessels with multiple BoP units ensures that partial operation can continue in the event of a failure, thereby minimizing downtime.

By contrast, automotive BoPs are subject to strict constraints on weight and space, which drive the need for high power density. This often requires sacrificing some efficiency to extract more power from compact systems. Automotive fuel cells commonly operate at current densities up to 2.5 A/cm^2, while maritime stacks typically run closer to 1 A/cm^2 to improve efficiency. When looking at a fuel cell polarization curve, one can see higher current density results in greater losses and lower cell voltage, which in turn reduces efficiency [17]. Automotive systems typically target power outputs around 100 kW and must accommodate frequent and rapid changes in load. As a result, BoP components for vehicles must be capable of fast ramp-up and ramp-down to ensure responsive performance under dynamic driving conditions.

2.2.2. Differences in fuel cell design

For maritime applications, fuel cell stacks often utilize thicker membranes to prioritize durability and robustness. While these membranes improve resistance to wear and failure, they also introduce higher internal resistance, which reduces cell voltage and overall system efficiency [13]. Unlike automotive systems, maritime fuel cells typically operate under steady loads for extended periods, making rapid start-up times less critical. Furthermore, the mechanical design of maritime stacks must account for different vibration and shock profiles, requiring different structural considerations. As a result, key differences in fuel cell design between the two sectors include power density, expected operational lifetime, number of cycles, and the importance of minimizing weight.

2.3. System comparison

This report compares several hydrogen loop configurations, including two based on real-world projects familiar to the author, while the remaining configurations are conceptual and not directly tied to existing systems. The first reference system is installed on the H2 Barge 1, an inland shipping container vessel developed by Future Proof Shipping. This vessel features three BoPs, each delivering a net

power output of 275 kW using Nedstack FCS 13-XXL fuel cells [18]. The second system is a prototype hydrogen-powered race car developed by the student team Forze Hydrogen Racing. It uses two BoPs, each rated at 120 kW, built around EKPO NM-12 Single stacks [19]. These two applications differ significantly, not only in power demand and operating conditions, but also in usage profiles. For example, total runtime is a critical design factor in maritime systems, whereas it is of minimal concern for the race car. Figure 2.1 illustrates both projects.

(a) H2 Barge 1

(b) Forze F9

Figure 2.1: Pictures of the H2 Barge 1 and Forze F9

Fundamentally, both the Forze race car and the H2 Barge 1 hydrogen systems operate on similar principles: hydrogen is stored in high-pressure tanks and reduced in two stages to the working pressure required by the PEM fuel cell. In both setups, unreacted hydrogen from the stack outlet is recirculated using a pump, and a purge valve is used to remove inert gases such as nitrogen that accumulate during operation.

Despite these similarities, there are several key differences in system design. First, the method used to regulate hydrogen pressure from the intermediate stage to the stack inlet differs: one system uses a passive pressure regulator, while the other employs an actively controlled proportional valve. Second, the design and placement of the recirculation pump and water separator vary. One system uses a liquid ring pump positioned before the water separator, while the other uses a blower placed after it. These differences are illustrated in the P&IDs shown in figure 2.2.

In addition to component differences, the fuel cell stacks themselves also operate under different strategies. The H2 Barge 1 system uses fixed hydrogen pressures for each power setpoint, whereas the race car's system is designed to increase pressure as the power demand rises. Furthermore, the maximum current density in the race car's stack is nearly three times higher than that of the maritime system, which leads to different efficiency and water management challenges.

This thesis focuses specifically on the two most impactful components in the hydrogen loop: the hydrogen supply and recirculation devices. Using the P&ID of the H2 Barge 1 as a baseline system, alternative configurations will be modeled by varying these components. Tubing and valve sizing, as well as stack characteristics, will reflect those of the H2 Barge 1 to maintain relevancy and allow validation with real world data. The aim of this study is to evaluate a range of supply and recirculation combinations under realistic maritime conditions to identify the most effective and robust hydrogen loop configuration for PEM fuel cell systems in marine applications.

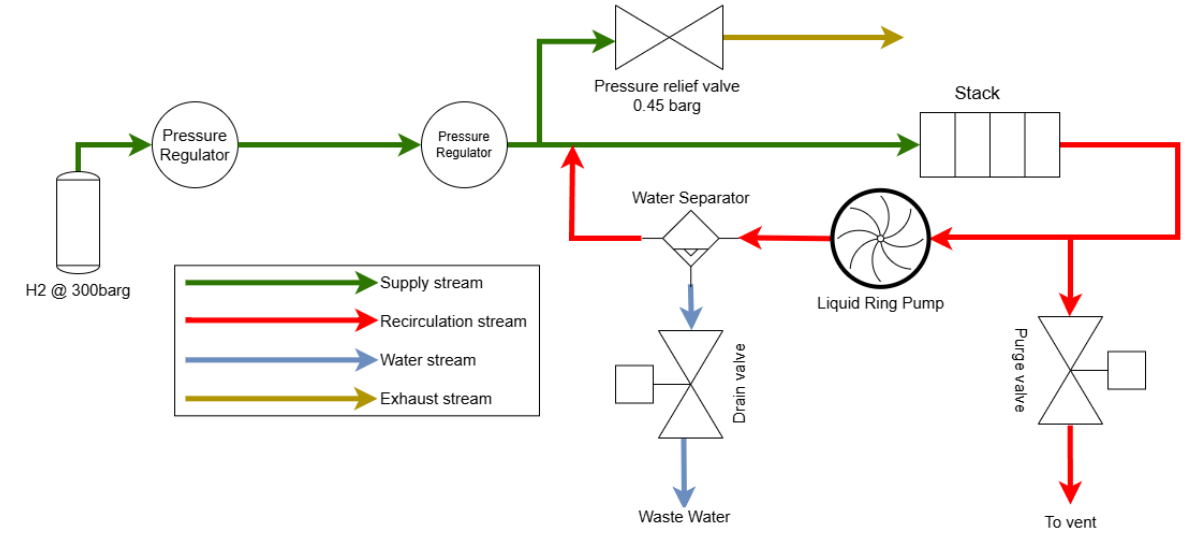

(a) H2 Barge 1 P&ID

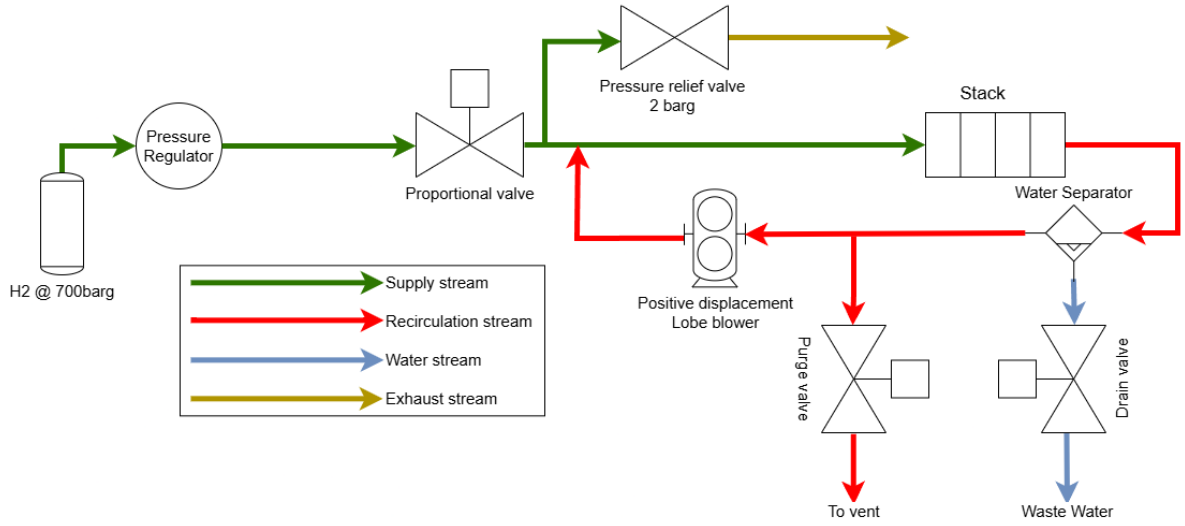

(b) Forze F9 P&ID

Figure 2.2: P&IDs highlighting key differences in hydrogen loop component placement between H2 Barge 1 and Forze F9

2.4. Hydrogen loop components and configurations

The next section introduces the key components that make up a hydrogen loop in a PEM fuel cell Balance of Plant. Each supply, recirculation, and auxiliary component is described in terms of its function, operating principles, advantages, and limitations. Finally, different combinations of these components are assembled into twelve distinct system configurations, which form the basis for the performance analysis presented in later chapters.

2.5. Stack

This master's thesis focuses on the FCS 13-XXL fuel cell stack developed by Nedstack. The BoP comprises of 32 of these stacks, in parallel, delivering a total power output of 300 kW at 145 A. At this operating point, hydrogen consumption is approximately 4.7 g/s and the stoichiometry should be at least 1.25. The anode operates at a fixed pressure of 250 mbar. The inlet temperature should be between 50 °C and 60 °C, and relative humidity between 50% and 80% with respect to coolant inlet temperatures (62 °C) [18].

2.6. Water and nitrogen crossover

Theoretically, all water generated in a PEM fuel cell is produced at the cathode. In practice, however, water crossover between the cathode and anode occurs in both directions. There are three primary mechanisms responsible for this transport across the membrane. The first is *electro-osmotic drag*, in which protons moving from the anode to the cathode carry water molecules with them. The second is *diffusion*, driven by the concentration gradient between the water-rich cathode and the typically drier anode. The third is *convection*, caused by a pressure gradient across the membrane [15].

Together, these mechanisms typically result in 10–40% of the water produced at the cathode crossing over to the anode. For the fuel cell stack considered in this study, NedStack estimates a water crossover of approximately 20–30%. This crossover influences overall system performance and component longevity: excess liquid water in the anode loop can lead to increased pressure drops, reduced component efficiency, and accelerated wear. At the same time, a certain degree of water crossover is beneficial, as it helps maintain adequate humidity in the hydrogen loop, which is essential for proper membrane hydration and long-term stack performance.

The porous nature of the fuel cell membrane permits gas crossover between the anode and cathode compartments [17]. While crossover of oxygen and hydrogen is undesirable, since it reduces efficiency due to fuel loss and, in extreme cases, may pose a safety risk due to the potential for local combustion, these gases react with each other and thus do not accumulate within the system. In contrast, nitrogen that crosses from the cathode to the anode accumulates in the hydrogen loop. This buildup blocks active surface area within the stack, leading to a reduction in cell voltage. Additionally, the presence of nitrogen increases the pressure drop across the loop, thereby raising the power consumption of the recirculation pump. However, because nitrogen crossover is difficult to quantify precisely and is considered negligible by the stack manufacturer, it has been excluded from this model.

2.7. Supply components

The purpose of the supply component is to apply enough hydrogen to the stack for the electrochemical reaction. An ideal supply device would supply this hydrogen at the right pressure and mass flow. Various methods exist for delivering hydrogen from the storage tanks to the fuel cell stack. Typically, a pressure regulator reduces the hydrogen pressure from the storage pressure (20-700 bar) to an intermediate pressure (5-20 bar), after which various methods can be employed to further reduce the pressure to the stack's operating pressure. Several different devices are used for this application and those are discussed below, furthermore, their benefits and drawbacks are discussed.

2.7.1. Pressure regulator

The pressure regulator (PR) controls the pressure supplied to the stack by adjusting an orifice in response to the outlet pressure. The orifice size then controls the flow, as can be seen in figure 2.3. A key drawback of using a pressure regulator is that it maintains a fixed outlet pressure. Although the set pressure can be adjusted, this process requires the system to shut down and careful calibration, making it unsuitable for dynamic adjustments during operation.

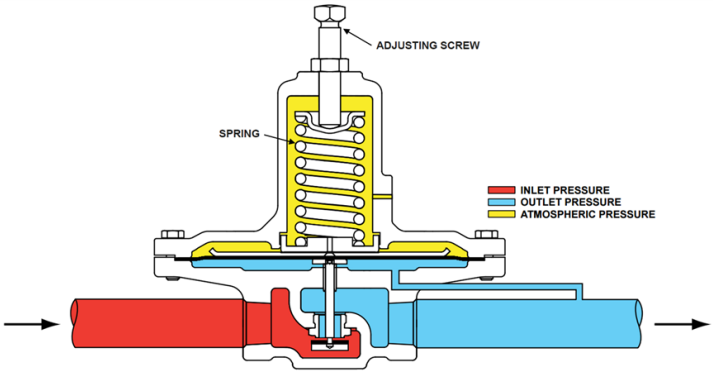

Figure 2.3: Schematic showing the working principle of a pressure regulator [20]

A typical flow curve for a pressure regulator can be seen in figure 2.4 taken from [21]. One can see that when the flow starts, there is a drop in outlet pressure, this is mainly caused by mechanical friction inside the pressure regulator. When setting the pressure regulator, it is set at a flow that has to overcome this lockup. With increasing flow, the outlet pressure drops, this is called droop. Near the end of the flow curve, choked flow happens and significantly reduces outlet pressure, this region should be avoided.

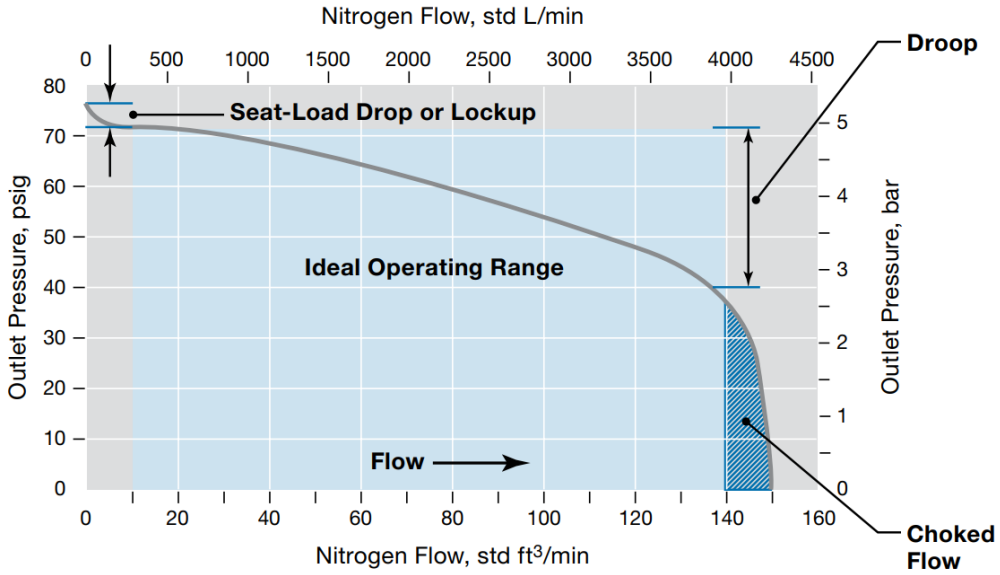

Figure 2.4: Typical flow curve of a pressure regulator [21]

2.7.2. Proportional valve

The proportional valve (PV) operates by adjusting the position of a plunger, which in turn varies the size of an orifice, thereby controlling the mass flow. The proportional valve can thus control the mass flow and with this, the pressure. The working principle can be seen in figure 2.5. As it is an active component, it can be controlled for a range of different outlet pressures and thus vary the inlet pressure of the stack based on its setpoint, allowing for more flexibility. Proper control and tuning are required for effective operation. A key consideration is the inlet pressure of the proportional valve, which must be at least twice the outlet pressure to ensure choked flow. Unlike pressure regulators, where choked flow is typically avoided, it is desirable in the case of proportional valves. Under choked conditions, the flow through the orifice becomes independent of downstream pressure and depends solely on the upstream pressure and opening of the orifice, simplifying flow control. However, this requirement imposes additional constraints on the minimum supply pressure.

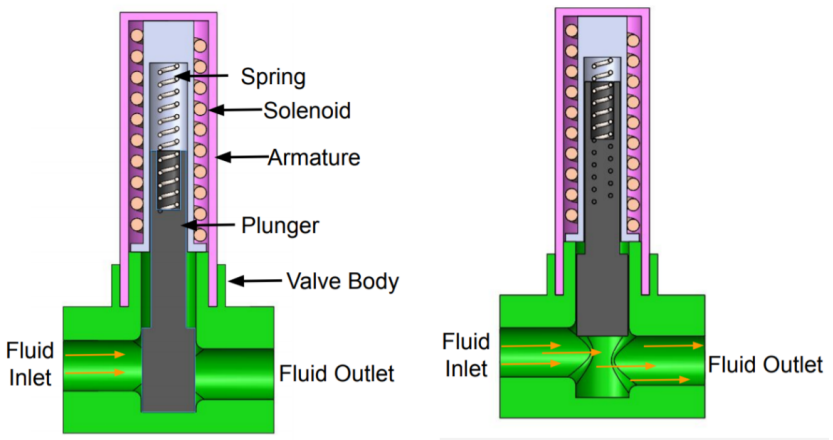

Figure 2.5: Schematic of a closed (left) and open (right) proportional valve [22]

2.7.3. Mass flow controller

A mass flow controller (MFC) operates in a manner similar to a proportional valve, but with integrated feedback control. Functionally, it consists of a mass flow meter followed by a proportional valve, as illustrated in figure 2.6. The mass flow meter continuously measures the flow rate, and this signal is used to adjust the opening of the proportional valve in real time. This configuration provides a straightforward and reliable method for controlling mass flow.

One of the key advantages of a mass flow controller is its simplicity: it is typically supplied as a complete unit, including control electronics, and is pre-calibrated by the manufacturer. This reduces the need for custom tuning and integration effort. However, a notable limitation is that it regulates only mass flow, not pressure. As a result, while it maintains a certain mass in the loop, it cannot compensate for changes in system pressure caused by variations in temperature or humidity. Consequently, system pressure may fluctuate even when mass flow remains constant.

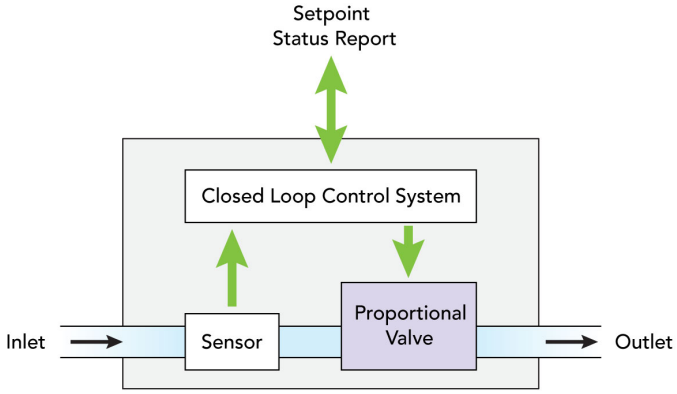

Figure 2.6: Schematic of a mass flow controller and its control system[23]

2.7.4. Injectors

Injectors provide another method for delivering hydrogen to the fuel cell by rapidly pulsing hydrogen to maintain a stable pressure. The duty cycle of the injector can be controlled to regulate the amount of mass flow to the fuel cell. This allows precise mass flow control and gives the system a quick dynamic response to changes in setpoint or changes in operating conditions. However, the injector has to be properly calibrated for it to be accurate. This might make this solution costly compared to the others. Injectors also have the ability to pulse hydrogen, which could lead to advantages in combination with an ejector [24].

2.8. Recirculation components

The function of the recirculation device is to recirculate the unreacted hydrogen. This will also recirculate the humidity and water, which will humidify the supply stream. Furthermore, the recirculation device should remove excess water from the fuel cell to prevent flooding. Together with the supply device, they can supply hydrogen to the fuel cell at the right pressure, temperature, humidity, and mass flow. Below, several options for recirculation are discussed. Both the liquid ring pump and the blower are positive-displacement pumps, meaning that they compress a volume to generate pressure and flow. Centrifugal pumps are not discussed as the low molecular weight of hydrogen makes them unfeasible [3].

2.8.1. Liquid ring pump

A liquid ring pump (LRP) operates using a liquid, typically water, as both a sealing medium and a lubricant, as shown in figure 2.7. In the context of a PEM fuel cell system, this sealing liquid can often be supplied by the fuel cell itself through its water production. One of the key advantages of a liquid ring pump is its ability to handle gas streams with significant droplet content, making it particularly suitable for fuel cell Balance of Plant applications where the stream can consist of significant water.

Another benefit of this design is its potential for thermal management: by controlling the temperature of the sealing liquid, the gas temperature can be indirectly regulated. However, a water separator is required downstream of the pump to remove both the water generated by the fuel cell and the sealing liquid carried over during operation. As a positive displacement device, the flow rate of a liquid ring pump is primarily determined by its rotational speed rather than the pressure differential across it. A known limitation is that it requires a minimum rotational speed to sustain the centrifugal force needed to maintain the liquid ring [25]. Additionally, liquid ring pumps generally consume more power than dry-running alternatives, as they must circulate both the process gas and the sealing liquid.

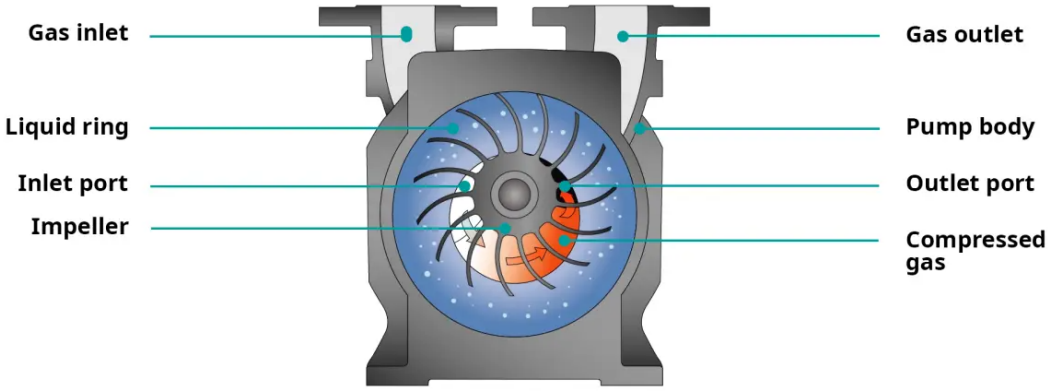

Figure 2.7: Schematic of a liquid ring pump [26]

2.8.2. Blower pump

A roots-style pump, commonly referred to as a hydrogen recirculation blower, is a type of positive-displacement pump. Unlike a liquid ring pump, it uses mechanical seals and does not rely on a liquid for sealing or lubrication. As a result, it is mechanically more simple and does not require additional plumbing for water supply. However, this design also limits the pressure ratio it can achieve, as mechanical seals are less effective at sealing under high differential pressures. Fortunately, most PEM fuel cell systems operate at relatively low pressures, making this limitation acceptable. The working principle of a roots-style blower is illustrated in figure 2.8. To protect the pump from water-induced damage, a water separator is typically placed upstream to remove any liquid droplets present in the gas stream. During operation, gas compression within the blower causes a temperature increase, which may raise vapor concentrations. While this can assist in water management, it also risks drying the membrane if not properly controlled, potentially impacting fuel cell performance and durability.

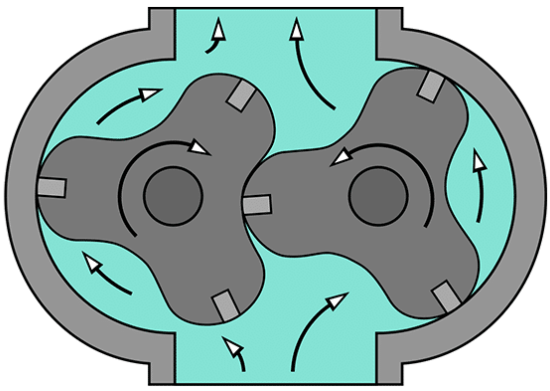

Figure 2.8: Schematic of a roots style blower [27]

2.8.3. Ejector

An ejector is a promising candidate for hydrogen recirculation in PEM fuel cell systems due to its ability to operate without external power. It utilizes the energy of the pressurized hydrogen supply to drive the recirculation of unreacted hydrogen. In an ejector, high-pressure hydrogen passes through a nozzle, accelerating to high velocity and creating a low-pressure zone downstream. This low-pressure region entrains the recirculated hydrogen from the anode outlet, enabling recirculation flow. A schematic representation of the ejector is shown in figure 2.9.

The performance of an ejector is highly sensitive to the precise geometry of its nozzle and diffuser, which determine the level of entrainment generated for a given primary flow rate. Achieving optimal performance requires careful sizing and tuning, which can be time-consuming. Moreover, any disturbance in the recirculation stream, such as increased pressure drop or water droplets, can disrupt suction and halt the recirculation process entirely.

Despite these challenges, ejectors offer several notable advantages: they contain no moving parts, are highly reliable, require minimal maintenance, and offer a long operational life. However, their operation is inherently coupled to the flow rate of the primary (supply) stream, which limits control flexibility. Specifically, ejectors do not allow independent adjustment of the hydrogen stoichiometry, which can be a constraint in systems requiring more flexibility. A major limitation is their reduced effectiveness at low power setpoints, where the primary hydrogen flow is insufficient to generate adequate suction. This can lead to issues such as hydrogen starvation or flooding in the recirculation loop. One mitigation strategy is to increase the purge rate to boost flow through the stack, although this comes at the cost of efficiency. Alternatively, hybrid configurations can be employed, in which a blower supplements the ejector at low loads, while the ejector takes over at higher power levels. Despite these limitations, ejectors remain an attractive solution in systems prioritizing simplicity, reliability, and energy efficiency.

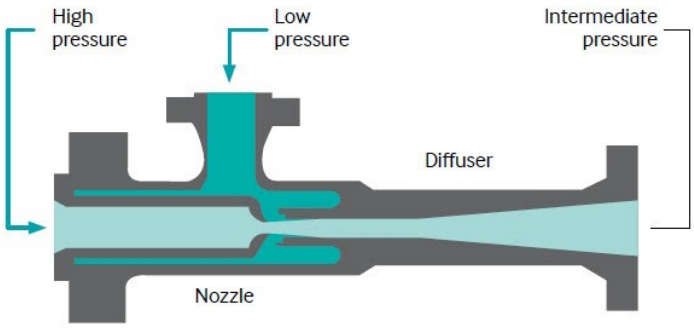

Figure 2.9: Schematic of an ejector [28]

2.9. Auxiliary components

Besides the components that supply and recirculate the hydrogen, several other components are needed for the BoP to function correctly.

2.9.1. Purge valve

A purge valve is used to remove unwanted gases or fluids from the hydrogen recirculation loop. These may include nitrogen that crosses over from the cathode side or impurities present in the supplied hydrogen. Since it is not possible to selectively purge only the contaminants, a portion of hydrogen is inevitably lost during the purge process. As a result, an effective purge strategy has a direct impact on both fuel utilization and overall system efficiency. Frequent or continuous purging helps maintain a high hydrogen concentration in the anode loop, which supports higher cell voltages and reduces pressure drop. This, in turn, can lower the power consumption of the recirculation pump. However, excessive purging leads to significant hydrogen losses, reducing fuel efficiency. Therefore, a careful balance must be struck between maintaining gas purity and minimizing hydrogen waste.

Two types of purge valves are commonly used: a discontinuous on/off valve and a continuously controlled valve [3]. A continuous purge involves a constant bleed typically around 3% of the hydrogen

flow, as suggested by simulation studies [29]. Purge strategies can be controlled based on various parameters, such as cell voltage, hydrogen concentration, or a predefined timer [29], allowing for adaptive optimization of system performance.

2.9.2. Water separator

Liquid water must be removed from the hydrogen stream to prevent flooding of the fuel cells, reduce pressure drop, and protect components that are not designed to handle liquid water. In the case of the liquid ring pump, the water it uses in its ring also needs to be separated. Separation can be done in several ways, the most common in BoPs are gravity separators, cyclone separators, or condensate traps. Gravity separators work by slowing down the gas stream and allowing the water droplets to fall down and be drained. This is a very simple solution with a low pressure drop, but it might not have the highest separation efficiency. Cyclone separators work by using centrifugal force to separate the liquid water from the hydrogen, as their densities are significantly different. Condensate traps work by having a heat exchanger cool down the hydrogen stream, allowing the humidity to condense and separate.

2.10. Configurations

Several of these previously discussed components can be used together, each system needs at least one supply device and one recirculation device. Typically, only one of each device is used with the exception of an ejector and pump hybrid. This research will concern three different supply options, a pressure regulator, a proportional valve, and a mass flow controller. The injector will be omitted because its pulsing effect will not be able to be captured in this model, so a proper comparison cannot be done. Four different recirculation options will be investigated, a liquid ring pump, a blower, an ejector, and an ejector-blower hybrid. These combinations result in twelve configurations, two of which are the same as the ones discussed in paragraph 2.3, and all of them can be seen in appendix A.

2.11. Reliability considerations

Reliability is a critical factor in the design of hydrogen loop configurations. One of the main challenges limiting the widespread adoption of PEM fuel cell applications is their relatively low reliability [30]. Figure 2.10 shows that the BoP is significantly more limiting to the lifetime of the fuel cell system than the fuel cell stack itself. This figure is taken from a paper that made a framework to determine the lifetime of fuel cell systems [31].

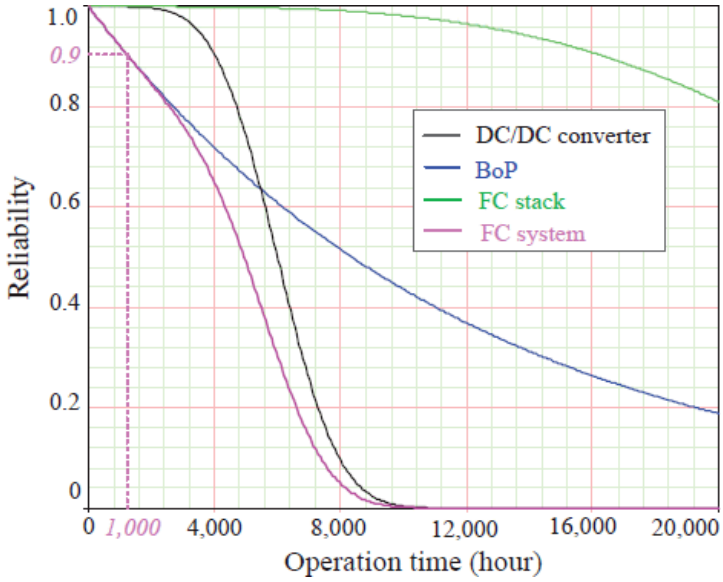

Figure 2.10: Subsystem-level and system-level reliability of a PEMFC system [31]

This lack of reliability can be explained by a couple of reasons. Firstly, even though most of these components have been employed before for other uses, they have not been in development for long

periods of time for applications in BoPs and might thus not be fully understood yet. Secondly, hydrogen itself is a very small molecule, which means that any component that handles hydrogen needs to be very leak-tight. This means reliance on proper sealing and tight tolerances, which are both subject to wear and relatively little wear is needed for it to cause leakages or other issues. Lastly are contaminants, like oil for lubrication or particles that get into the system. As the system is designed for hydrogen, tolerances are tight, so any contaminants can make the components wear significantly quicker. Besides this, most contaminants will also damage the fuel cell itself.

3

Dynamic Modeling Approach and Methods

To enable a good comparison of hydrogen loop configurations, a custom model was developed in MATLAB Simulink. This model is unique in its ability to capture time-dependent behaviors such as startup transients, humidity build-up, and component response delays. It incorporates physics interactions, like pressure, flow, temperature, and two-phase effects, while allowing component-level parameterization and validation against real-world maritime data. This chapter describes the modeling framework, including the governing physical principles and component-level implementations used to simulate pressure, flow, temperature, humidity, and phase changes within the hydrogen loop. The chapter concludes by outlining the methods used for configuration scoring and performance evaluation, providing the basis for the comparative analysis presented in the next chapter.

3.1. System overview

The system is modeled as a network of volumes, flow resistances, and components. The layout and components are based on the P&ID shown in figure 2.2a, primary components include the hydrogen supply device, fuel cell stack, purge valve, recirculation device, and water separator. Mass flows between volumes through flow resistances, and each volume additionally accounts for phenomena such as temperature, relative humidity, and species concentration. Heat transfer through the piping is included in temperature calculations to account for thermal interactions with the environment. The model can be seen in appendix B.

3.2. Governing physics and equations

3.2.1. Pressure

The pressure within each volume is computed using the ideal gas law. The use of the ideal gas law is justified by the relatively low operating pressures and temperatures. The amount of mass per species in each volume is calculated via time integration of the net mass flow into and out of each volume. This is applied separately to hydrogen and water vapor, and the total pressure is obtained by summing their respective partial pressures.

3.2.2. Flow

Flow between volumes is calculated based on the pressure difference between them, using the Darcy-Weisbach equation. Since this equation expresses pressure drop as a function of flow velocity, it is algebraically rearranged to solve for velocity as the output. To accurately represent the gas mixture comprising hydrogen and water vapor, the model calculates viscosity using Wilke's method, while density is determined separately based on the ideal gas law. In addition to these gaseous species, the presence of liquid water requires the use of two-phase flow correlations. Specifically, the Lockhart-Martinelli method is employed to account for the increased pressure drop associated with simultaneous

gas-liquid flow. Once the flow velocity is determined, it is used to calculate the corresponding mass transfer between volumes. All underlying equations and assumptions are detailed in appendix C.

3.2.3. Temperature

Temperature is calculated at each volume for both the fluid stream and the tube wall. Thermal modeling includes convective heat transfer between the fluid stream and the tube wall, conduction through the wall, and free convection to the ambient environment. Convective heat transfer coefficients are determined using internal and external Nusselt number correlations, based on the local flow regime. It is assumed that hydrogen, water vapor, and liquid water within the stream share the same bulk temperature. Additionally, phase change due to condensation and evaporation significantly affects thermal behavior. These effects are accounted for and the resulting heat is appropriately distributed between the fluid stream and the wall. A detailed description of all thermal and phase-change equations is provided in appendix C.

3.2.4. Relative humidity

As discussed in paragraph 3.2.1, there are three mass balances, the mass balance of the vapour is used to calculate the vapour pressure. The saturated vapour pressure is calculated with the Arden-Buck equation, see equation 3.1 where T is the temperature in Kelvin and p the partial pressure [32]. This equation gives an good approximation of the saturated vapour pressure. The relative humidity is then calculated with equation 3.2.

$$p_{sat} = 611.21exp\left[\left(18.678 - \frac{T - 273.15}{234.5}\right)\left(\frac{T - 273.15}{T - 16.01}\right)\right] \tag{3.1}$$

$$RH = \frac{p_{vapour}}{p_{sat}} \tag{3.2}$$

3.2.5. Evaporation and condensation

Evaporation and condensation are key processes within the hydrogen loop, significantly influencing both humidity and temperature throughout the system. These phase changes are driven by temperature changes, which affect the saturation pressure and enable mass transfer between vapor and liquid phases. In the model, phase change rates are dynamically computed using mass transfer correlations based on concentration gradients and local flow conditions. The mass transfer coefficient is determined using Sherwood number correlations, while vapor saturation pressure is calculated with the Arden-Buck equation 3.1. The associated latent heat effects are included in the energy balance, ensuring that phase change impacts both heat and mass dynamics realistically. A complete formulation of the equations and modeling approach is provided in appendix C.

3.3. Components

3.3.1. Stack

The stack is modeled as a simple consumer of hydrogen. Based on the current setpoint, the consumption mass flow can be calculated with equation 3.3, where I is the stack current, n_{cells} is the number of cells, M_{H_2} is the molar mass of hydrogen, and F is the Faraday constant [16]. To prevent flooding, a minimum flow rate of 1888 Nl/min is enforced by increasing recirculation when necessary. Water crossover from cathode to anode is included in the model and assumed to be 20-30% of the produced water. The total water production rate is calculated using equation 3.4 [16].

$$\dot{m}_{\text{H}_2,\text{consumed}} = \frac{In_{\text{cells}}M_{\text{H}_2}}{2F} \tag{3.3}$$

$$\dot{m}_{\text{H}_2\text{O},\text{produced}} = \frac{In_{\text{cells}}M_{\text{H}_2\text{O}}}{2F} \tag{3.4}$$

Due to the high thermal inertia of the stack, the assumption is made that the stream leaving the stack has the same temperature as the coolant. Nitrogen crossover is not modeled as it is dependent on many factors like humidity of membrane, partial pressure on both sides of the membrane, temperature,

membrane material characteristics, some of which are not known, and the amount is expected to be very small, thus, the overall effect on the system will be minimal.

3.3.2. Pressure relief valve

In case of an overpressure in the loop, a pressure relief valve opens to let out the excess pressure. In this system, this valve is set at 450 mbar. This valve is modelled as a simple valve, the more pressure there is, the further this valve opens. When below 450 mbar it closes again.

3.3.3. Water separator

As little is known about the actual water separator used in the BoP, characteristics of another water separator are used. In figure 3.1, one can see that the efficiency drops with increasing flow rate and the pressure drop increases, this is to be expected and thus a good alternative to use in the model. To adjust it to the system, it was assumed that three of these would be in parallel, meaning the flow gets divided over them.

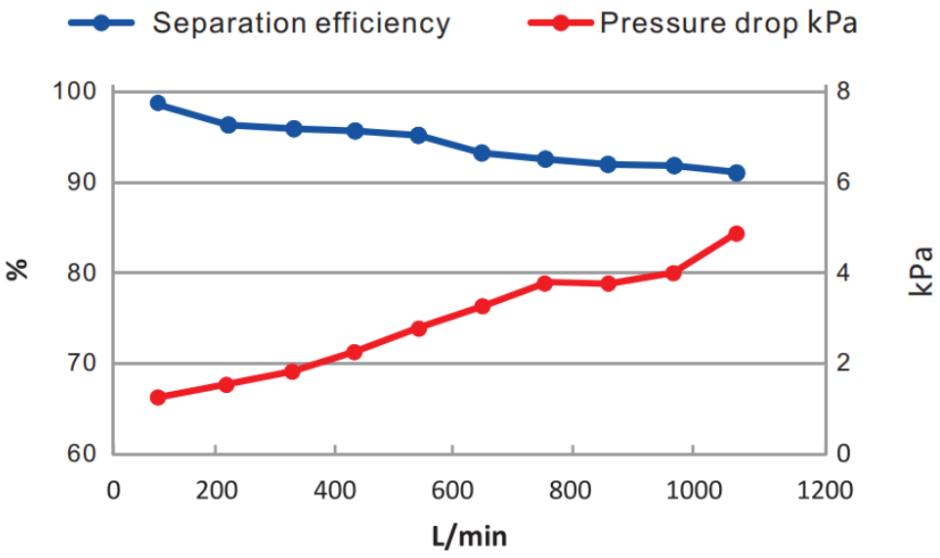

Figure 3.1: Water separator efficiency and pressure drop at increasing flow rate [33]

3.3.4. Purge valve

The purge valve is a simple on/off valve that is open 90% of the time, cycling with a period of one second to minimize pressure fluctuations in the system. The valve's flow rate at a known pressure and temperature is used to determine its Kv value, a flow coefficient that quantifies how much fluid passes through the valve for a given pressure drop. This Kv value is then used with equation 3.5 to calculate the flow rate under current system conditions, where p is the pressure inside the system p_{amb} the ambient pressure, ρ the density of the mixture, and T the temperature [34]. The resulting flow can be split into hydrogen and vapor mass flows based on the local gas composition.

$$\dot{V}_{purge} = 514Kv\sqrt{\frac{(p - p_{amb})p_{amb}}{\rho_{mixture}T}} \tag{3.5}$$

In the case of an ejector-based system, achieving sufficient flow through the stack at low load setpoints is not possible using the ejector alone. To address this limitation, an additional, larger purge valve is employed alongside the standard purge valve. This setup allows enough hydrogen to pass through the stack to prevent flooding. While this approach is highly inefficient, resulting in significant hydrogen losses, it is necessary to safeguard the health and longevity of the fuel cell stack.

3.3.5. Pressure regulator

The flow curve of the pressure regulator is known and can be seen in figure 3.2. This is implemented in a lookup table. Here, the outlet pressure is the input to the lookup table, and the mass flow is the output. Inertia in the pressure regulator is assumed to be minimal and thus ignored. The inlet pressure of the pressure regulator is assumed to be constant, as the volume before the pressure regulator is large.

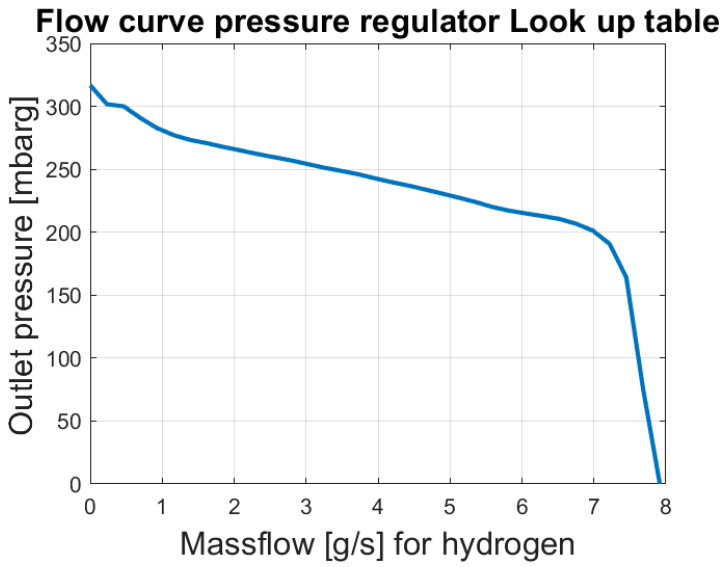

Figure 3.2: Flow curve of the pressure regulator used in the model

3.3.6. Proportional valve

The proportional valve is a simple valve that, based on its input, opens a certain amount. This changes its Kv value and, thus the flow rate. The flow rate can be calculated with equation 3.6, [34]. If the flow is not choked, equation 3.5 should be used. One can check if the flow is choked when the inlet pressure is more than twice the outlet pressure of the valve. The proportional valve will be based on a Bürkert type 6223, with a Kv of 1.4 m^3/h [35]. The proportional valve also shows hysteresis effects, as can be seen in figure 3.3, these effects have also been taken into account in the model. A PID controller will control the opening of the valve based on the stack inlet pressure.

$$\dot{V}_{PV} = \frac{257 p_{in} Kv}{\sqrt{\rho T}} \tag{3.6}$$

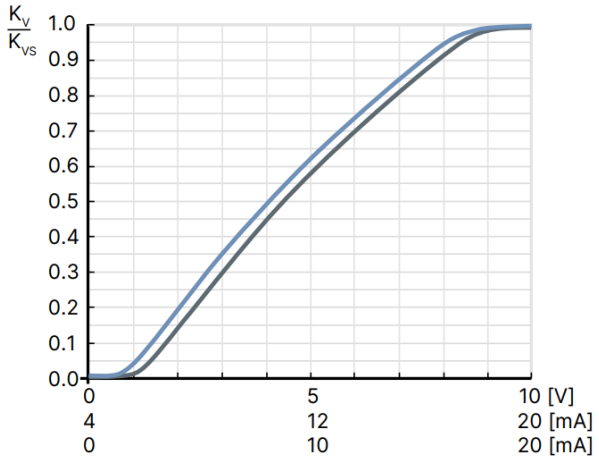

Figure 3.3: Hysteresis of a proportional valve

3.3.7. Mass flow controller

The mass flow controller uses the same governing equations as the proportional valve. However, it is controlled based on the measured mass flow rate. A PID controller adjusts the valve opening to maintain the desired mass flow.

3.3.8. Liquid ring pump

The pump map for the liquid ring pump is known and serves as a key reference. The model uses the pressure rise over the pump, derived from this map, to calculate the corresponding flow. The map can be seen in figure 3.4. A simple PID controller will control the pump's setpoint.

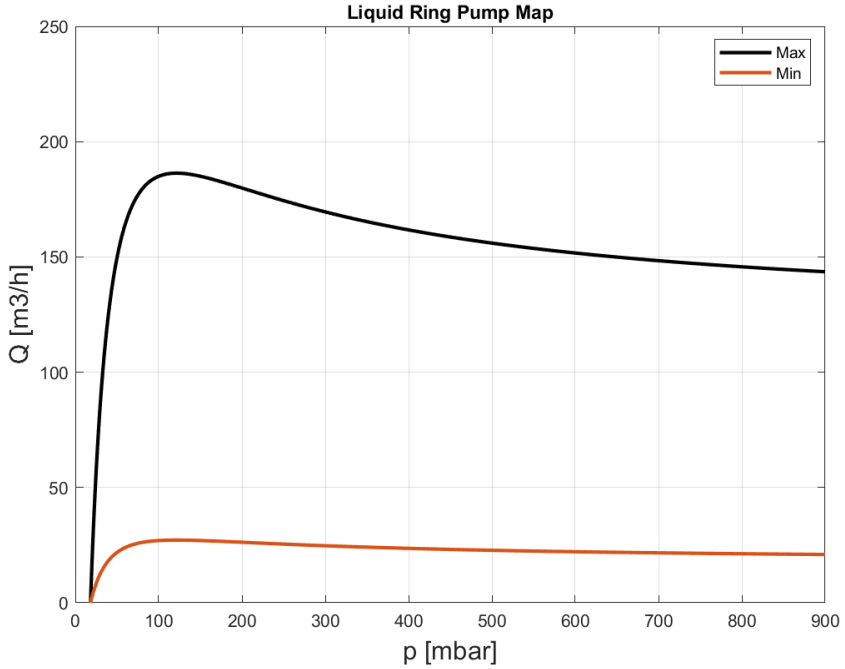

Figure 3.4: Flow rate and pressure rise of the liquid ring pump at minimum and maximum setpoint

The pump's inertia is modeled as a rotating cylinder with an inner steel ring and an outer water ring. The power and RPM of the motor attached to the pump is known and is thus modeled. Furthermore, the pump has a minimum speed to maintain the liquid ring, based on the geometry, a minimum speed of 14.59% was found.

3.3.9. Blower

For the inspiration of the blower, a 24 URAI was taken due to a lot of information being available and suitable for the requirements of the system [36]. The pump map, power, and temperature rise were available and were modified for the mixture going through. The inertia was modeled based on the sizing available.

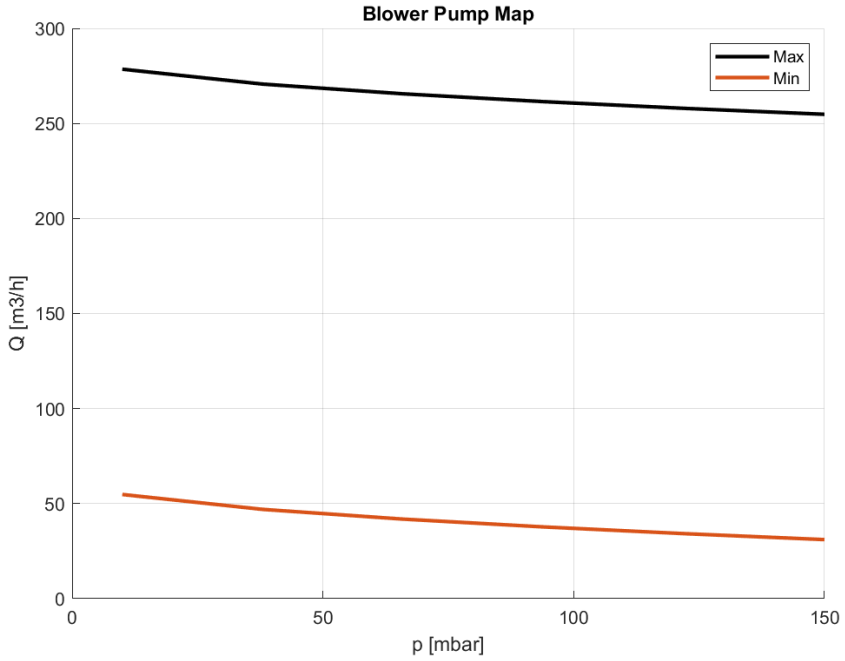

Figure 3.5: Flow rate and pressure rise of the blower pump at minimum and maximum setpoint

3.3.10. Ejector

To model an ejector, it is essential to predict the entrainment ratio, defined as the ratio of secondary to primary mass flow, as shown in equation 3.7, where $\dot{m}$ denotes the mass flow rate [37]. Once the entrainment ratio is known and the primary mass flow is specified, the secondary mass flow can be calculated directly.

The entrainment ratio under critical flow conditions is determined using the methodology proposed by Chen et al. [37]. For subcritical operation, the entrainment ratio is interpolated based on the calculated start and end points of subcritical behavior and the current backpressure, as illustrated in figure 3.6.

This calculation is performed across a range of primary pressures, secondary pressures, back pressures, and hydrogen concentrations. The resulting data is stored in a four-dimensional lookup table, which is used within the model to dynamically determine ejector performance under varying operating conditions.

$$\omega = \frac{\dot{m}_{secondary}}{\dot{m}_{primary}} \tag{3.7}$$

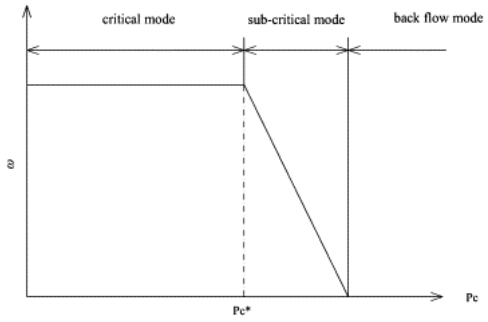

Figure 3.6: Entrainment ratio vs back pressure in different flow regimes [37]

The ejector geometry was sized based on the maximum required hydrogen supply flow at full stack load and elevated temperature. To determine the diameter of the constant-area mixing section, a design

ratio of 3.135 was applied, based on guidelines from [38], [39]. The final geometry parameters used in the model are listed below. The corresponding performance curve for the ejector is shown in figure 3.7.

- Throat diameter = 3.55 mm
- Nozzle exit diameter = 6.15 mm
- Constant area diameter = 11.13 mm

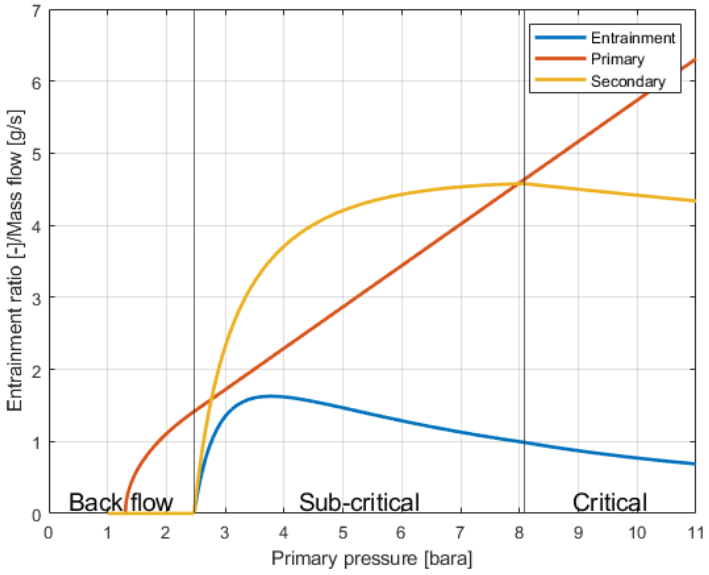

Figure 3.7: Performance curve of the ejector used in the model, in the different flow regimes

3.3.11. Ejector pump hybrid

In the hybrid configuration, the ejector and the pump are arranged in parallel, with valves directing flow through either device depending on the operating condition. Control is based on the stack load setpoint: when the load exceeds a defined threshold, the ejector is activated; otherwise, the blower is engaged. This arrangement enables efficient operation of the fuel cell system's Balance of Plant across the full range of the stack.

3.4. Validation

Model validation was conducted using operational data from the H2 Barge 1 system. Two datasets were available: a comprehensive dataset with limited sensor coverage, and a shorter dataset containing detailed measurements of the hydrogen loop. These datasets were used to compare model predictions and inform iterative refinements. Several model parameters were tuned to better align with the measured data. These include the ambient temperature, hydrogen supply temperature, and stack outlet temperature. Initially, the temperature rise across the liquid ring pump was assumed to be negligible. However, measurements showed a temperature increase of approximately 6 °C at high power, prompting a correction.

The pressure regulator's original flow curve was based on a 6 bar inlet pressure. However, measurements indicated an actual inlet pressure of 10 bar, necessitating scaling the flow curve. Additionally, the regulator's set pressure was observed to be higher than expected and was adjusted accordingly. Figure 3.8 compares measured flow data with the adjusted regulator curve, showing the raw data and the midpoints for each bin to compare them to the flow curves. While figure 3.9 shows the final versus initial flow curves. A scaling factor for flow rate was also introduced to assess the impact of inlet pressure.

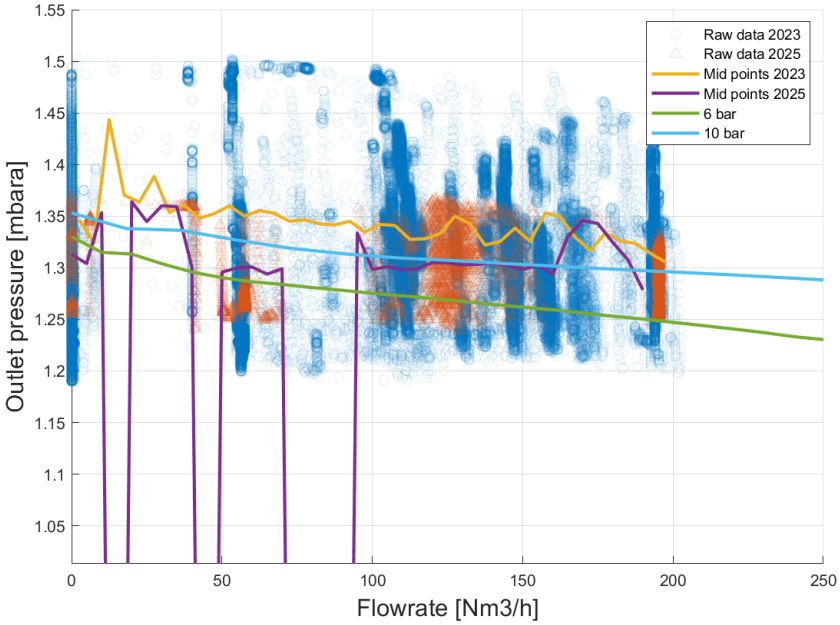

Figure 3.8: Data from the system on the ship compared to pressure regulator flow curve

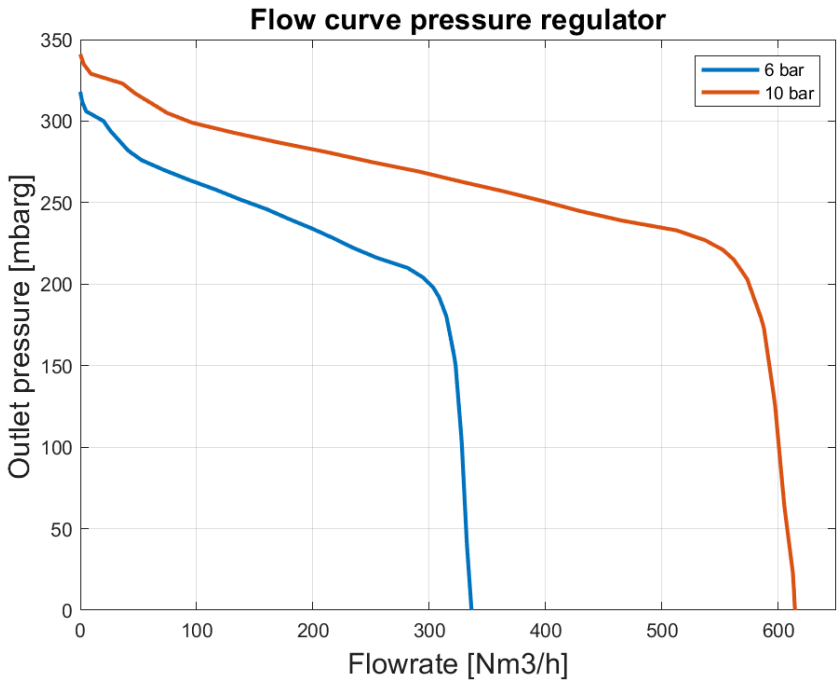

Figure 3.9: Pressure regulator flow curve altered to match the ship

The pressure drop across the stack was also refined based on experimental data. Using the large dataset, the hydrogen utilization was computed and used to adjust the purge valve's Kv value to match the measured utilization when the same load profile was simulated in the model.

It is important to note that differences in control strategies between the real ship system and the simulation influenced the validation process. For example, the purge duty cycle on the ship is dynamically controlled, whereas in the model it is implemented as a fixed value. Additionally, the hydrogen recirculation pump on the ship operates continuously at its maximum setpoint and, in practice, even exceeds the manufacturer's specified maximum RPM due to the characteristics of the motor used. In contrast,

the simulation employs a variable-speed setpoint for the pump. These operational discrepancies were taken into account during the validation phase. However, for the sake of standardized comparison across different configurations in this study, the simulation model was ultimately simplified to use idealized control logic.

Appendix E presents a side-by-side comparison of model outputs and experimental data. Most sensor readings show good agreement, with the largest discrepancy observed in the stack inlet temperature, which is consistently lower in the model. After an extensive investigation, no modeling error could be identified to explain this deviation. The most plausible explanation is a difference in sensor placement between the physical system and the modeled representation.

3.5. Evaluation metrics and test scenarios

This section outlines the methods used to evaluate and compare the performance of the twelve different hydrogen loop configurations, listed in appendix A. Each configuration undergoes a standardized set of tests, and is assessed based on key performance indicators (KPIs). After determining the working range of each configuration, some configurations might be dropped as they are not suitable for use and will take up time.

The first step is to determine the operational working range of each configuration. This is achieved by performing a load ramp test, where the stack load is gradually increased from 0% to 100% and then decreased back to 0%. A configuration is considered operationally viable across a load point if the following three criteria are met:

- Stoichiometry is above 1.25
- No excessive purging required
- Pressure relief valve remains closed

Excessive purging or activation of the pressure relief valve indicates loss of hydrogen or system instability, making the configuration unsuitable. Maintaining a stoichiometry above 1.25 is crucial to ensure sufficient hydrogen availability for the electrochemical reaction and to avoid flooding or starvation in the fuel cell stack.

Once the working range is established, each configuration is tested under various load conditions. Key performance indicators are defined to enable objective comparison between configurations. These KPIs include:

- Hydrogen utilization
- Recirculation device power consumption
- Hydrogen stoichiometry
- Minimum stack flow
- Stack inlet pressure
- Stack inlet relative humidity (relative to coolant inlet temperature)
- Stack inlet temperature

Target values for pressure, temperature, and relative humidity are defined by Nedstack [18], and each key performance indicator is scored individually based on its deviation from these targets. For instance, the stack inlet pressure has a target of 250 mbar; if the measured value remains within ±25 mbar of this target, it receives a full score. Larger deviations result in proportionally reduced scores.

Stoichiometry is evaluated using a binary scoring system: full points are awarded if the value is at least 1.25; otherwise, the score is zero. Minimum stack flow is scored in a similar fashion, with a

10% tolerance band around the required flow. Maintaining sufficient flow is critical to prevent flooding, a condition where water produced in the fuel cell is not effectively removed. This excess water can obstruct active cell areas, leading to local fuel starvation. Frequent flooding can accelerate membrane degradation and significantly reduce the fuel cell's operational lifespan.

Relative humidity should be evaluated relative to the coolant inlet temperature, as the coolant has the highest heat capacity compared to the hydrogen loop and air supply. It largely determines the fuel cell's operating temperature. When hydrogen enters the stack, it quickly reaches the stack temperature, approximately equal to the coolant temperature, due to the high surface area for heat exchange. As a result, its relative humidity changes rapidly upon entry, making the coolant temperature the relevant reference point for evaluating humidification. Relative humidity is scored asymmetrically, with higher penalties applied to over-humidification than to under-humidification. This reflects the greater risk of membrane flooding under excessive humidity conditions. Detailed scoring curves for each KPI are provided in appendix F.

Efficiency in this study is calculated using two factors. The first is hydrogen utilization, defined as the ratio of hydrogen consumed to hydrogen supplied. The second is the ratio of the power consumed by the recirculation device to the total power output of the fuel cell system. These two factors are multiplied to obtain the overall hydrogen loop efficiency, as shown in equation 3.8. It is important to note that this efficiency metric pertains only to the hydrogen loop and does not account for the electrochemical efficiency of the fuel cell itself, which typically operates at around 50%.

$$\eta = \left(\frac{H_2 \text{ consumed}}{\text{total } H_2 \text{ input}}\right) \times \left(1 - \frac{\text{recirculation power}}{\text{stack power}}\right) \tag{3.8}$$

These scores can be used to compare each system and come to a conclusion of which is the most suitable system. To make the comparison more meaningful, a weighted average is used. For the maritime sector, efficiency and lifetime are the most important factors. Thus, efficiency has a high weight, one big risk for the stack is flooding and fuel starvation, which can significantly decrease lifetime [40], thus they are weighted second. On the one hand, if the pressure is too high, the pressure difference over the membrane can be too much and there is an increased risk of damage to the membrane. On the other hand, a too low pressure can decrease cell voltage and thus efficiency and can also increase the amount of nitrogen and water crossover. Humidity and temperature can both increase the cell voltage and when they are too high, can cause damage to the stack. But the cathode side of the stack has more impact on this due to bigger flow, thus these are weighted lower. All the weights can be seen in table 3.1.

Table 3.1: Weights for the weighted average for each key performance indicator

	Percentage of total score
Efficiency	35%
Stoichiometry	15%
Minimum flow	15%
Pressure	17.5%
Humidity	10%
Temperature	7.5%

To say something about the transient behavior of each configuration, the response to a change in load will be recorded. This might not be the most relevant for maritime applications, as the expected load profiles are typically steady over long periods, but it is still valuable for assessing system robustness and identifying potential control challenges during start-up, maneuvering, or emergencies. Furthermore, in most BoPs, the compressor on the air side is the slowest component to ramp up or down and often limits the overall system response. The transient response will be evaluated by measuring how long it takes for the system to reach a new steady state in terms of pressure and stoichiometry. The test will consist of several load steps, both with and without a rate limiter provided by the stack manufacturer.

The robustness of the system will be investigated by changing ambient temperature, the temperature of the supply hydrogen and the amount of water crossover. These variables might change day to day for the system and seeing how robust the systems are to these changes can be important. They will be scored on how much they lose compared to a base scenario. Furthermore, the pressure of the supply hydrogen, upstream of the supply device, can fluctuate and a robust system should be able to handle the change in pressure and still be able to work on the complete range. They will be tested with a varying supply pressure that resembles real scenarios from the ship. And three scenarios with fixed pressure but at 8, 10 and 12 bar. Then, a relation between the inlet pressure and outlet pressure can be found. In an ideal system, these would be uncoupled, based on how coupled they are, the score is determined.

Steady load performance is also very important in maritime applications and is thus also scored and compared. Furthermore, the effect of an increased stoichiometry will be tested and compared, as this will increase the power draw of the pump but will also increase the humidity and temperature of the stream entering the fuel cell. Besides performance related criteria, other criteria like complexity and reliability will be considered. The will be done giving each component a score on several criteria, the configuration will then get the score of both devices combined.

4

Results and Discussion

This chapter presents the simulation results for the twelve hydrogen loop configurations introduced earlier, analyzing their performance under a range of operating conditions representative of maritime fuel cell applications. The simulations include a variety of test scenarios to evaluate both steady-state and dynamic behavior. These include fixed load points, gradual load sweeps, and transient load changes to assess responsiveness and robustness. Special attention is given to pressure and temperature stability, effectiveness of water management, and the ability of each configuration to maintain acceptable stoichiometry across the full load range. The results are discussed in terms of technical feasibility, energy efficiency, system reliability, and control complexity, providing insights into the trade-offs involved in selecting a suitable hydrogen loop design for maritime use.

4.1. Working range

The working range of each configuration was determined by ramping the load from 100% to 0% and back to 100% to assess any differences between upward and downward transitions. The results are summarized in table 4.1. Configurations 3 and 4 exhibited limited operating ranges and were therefore excluded from some of the subsequent tests.

The tests revealed that configurations using ejectors struggled to meet minimum operational requirements at low load setpoints. These limitations stem from the passive nature of ejectors and their lack of controllability. Ejectors require sufficiently high primary flow to generate the suction needed for recirculation. At low stack loads, this flow is inadequate, and compensating with excessive purging would lead to unacceptable hydrogen losses, rendering the approach impractical. When combined with a pressure regulator, the operating range is further reduced. A fixed inlet pressure constrains the hydrogen supply, limiting system operation to conditions where supply and consumption are closely matched.

Hybrid configurations address this challenge by combining an ejector with a blower. At low loads, the blower maintains the required recirculation flow, while at higher loads, the ejector can operate effectively, enabling reliable performance across the full range. This approach balances the need for high inlet pressure to drive recirculation with the goal of avoiding excess hydrogen consumption.

It should also be noted that in real-world BoP systems, other subsystems, such as the air supply or the fuel cell stack itself, can impose additional limitations on the achievable operating range. such as the air supply or fuel cell stack itself, may impose additional constraints on the operational range.

Table 4.1: Operating current range for each configuration during load ramping tests. The range indicates the lowest and highest stack currents at which stable operation was maintained.

Conf #	Devices	Working range [A]	
		Down ramp	Up ramp
1	Pressure regulator Liquid ring pump	145-0	0-145
2	Pressure regulator Blower	145-0	0-145
3	Pressure regulator Ejector	106-125	104-92
4	Pressure regulator Ejector blower hybrid	107-125	95-84
5	Proportional valve Liquid ring pump	145-0	0-145
6	Proportional valve Blower	145-0	0-145
7	Proportional valve Ejector	44-145	145-44
8	Proportional valve Ejector blower hybrid	145-0	0-145
9	Mass flow controller Liquid ring pump	145-0	0-145
10	Mass flow controller Blower	145-0	0-145
11	Mass flow controller Ejector	58-145	145-56
12	Mass flow controller Ejector blower hybrid	0-145	145-58

4.2. Load sweep

The performance score for the ramped and step load can be seen in table 4.2, the exact load profile can be seen in figure 4.1, this load profile spans 1800 seconds or 30 minutes. The load sweep tests provide a comprehensive view of each configuration's performance across various loads.

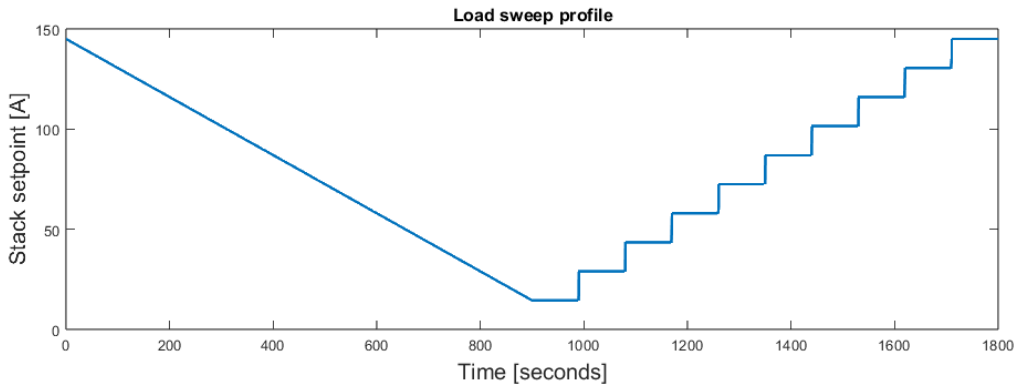

Figure 4.1: Load profile for the load sweep scenario, going from 100% to 10% and then going up in steps of 10%

Configurations utilizing only an ejector consistently scored lower in efficiency, primarily due to excessive purging at lower loads. Mass flow controllers struggled with pressure control, as they regulate mass flow rather than system pressure, failing to account for variations in temperature and humidity. Interestingly, the mass flow controller configurations achieved slightly higher scores for temperature and humidity. This is because the pressure in the system is higher with a mass flow controller, which increases

gas density, reducing the pressure drop across the stack. As the pump attempts to maintain a certain pressure drop, it increases speed, which in turn increases recirculation flow, temperature, and humidity. This effect is even more pronounced in fixed-load tests. The liquid ring pump, by humidifying the stream when not saturated and slightly increasing system temperature compared to the blower, scores marginally better for temperature and humidity but loses efficiency due to its higher power consumption.

Table 4.2: Scores for each configuration at several loads varying from 10% to 100%

Conf #	Devices	Efficiency	Stoichiometry	Minimum flow stack	Stack in pressure	Humidity wrt coolant inlet	Stack in temperature	Weighted score
1	Pressure regulator Liquid ring pump	95.77	100.0	100.0	94.9	95.3	98.0	97.01
2	Pressure regulator Blower	96.63	100.0	100.0	94.9	94.2	97.6	97.17
3	Pressure regulator Ejector							-
4	Pressure regulator Ejector blower hybrid							-
5	Proportional valve Liquid ring pump	96.20	100.0	100.0	100.0	94.4	97.7	97.94
6	Proportional valve Blower	97.04	100.0	100.0	100.0	92.7	97.2	98.02
7	Proportional valve Ejector	92.65	100.0	83.4	100.0	74.5	94.4	91.97
8	Proportional valve Ejector blower hybrid	97.13	100.0	100.0	100.0	87.5	95.5	97.41
9	Mass flow controller Liquid ring pump	94.66	100.0	100.0	2.9	96.3	98.7	80.67
10	Mass flow controller Blower	95.62	100.0	100.0	2.9	96.0	98.5	80.96
11	Mass flow controller Ejector	90.87	100.0	77.5	35.1	64.0	93.6	77.99
12	Mass flow controller Ejector blower hybrid	96.97	100.0	100.0	35.1	82.8	95.2	85.50

Figure 4.2 shows the stoichiometry traces for all recirculation options. Pumps maintain a fairly constant stoichiometry, while ejectors exhibit lower stoichiometry at higher setpoints and higher stoichiometry at lower setpoints. In the middle of the graph, where the load is lowest, stoichiometry rises as recirculation increases to meet minimum flow requirements.

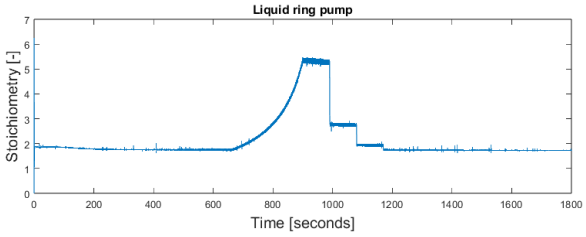

(a) Stoichiometry trace for the liquid ring pump

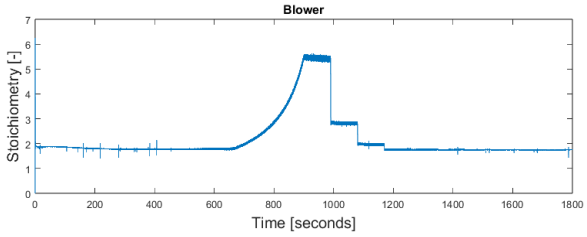

(b) Stoichiometry trace for the blower

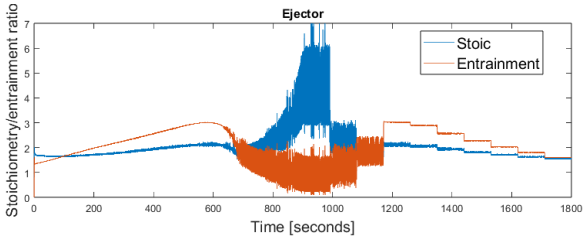

(c) Stoichiometry and entertainment ratio trace for the ejector

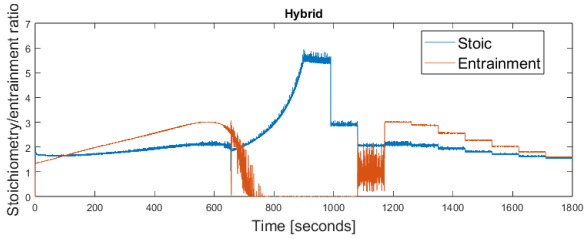

(d) Stoichiometry and entertainment ratio trace for the ejector-blower hybrid

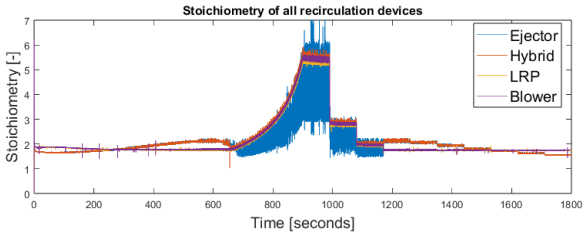

(e) All stoichiometry traces overlapper

Figure 4.2: Figures a and b show stoichiometry for the liquid ring pump and blower, both staying near 1.75 until the set-point drops and a higher flow is needed to meet the minimum flow requirement. Figures c and d display the ejector options, where stoichiometry initially rises with decreasing setpoint due to an increasing entrainment ratio, then drops sharply as the entrainment ratio falls and either the purge valve opens more or the blower activates. Figure e compares all options, showing that the ejector configurations start with lower stoichiometry at high setpoints but increase more gradually than the pump-based systems.

4.3. Fixed load

The same performance metrics used in the load sweep were also evaluated at fixed loads of 100% and 75%, which are representative of typical steady-state conditions during constant-speed sailing. The results are presented in tables 4.3 and 4.4.

At both fixed loads, configurations using ejectors performed significantly better than in the load sweep. This improvement is attributed to the alignment of these operating points with the ejector's optimal design range. Ejector and hybrid configurations show identical results under these conditions, as the blower in the hybrid setup remains inactive at higher loads and is only engaged during low-load operation. At 75% load, the pressure regulator–ejector combination operated acceptably, though its lack of active pressure control resulted in a low pressure score. These findings highlight that passive systems, such as those using ejectors or pressure regulators, can perform well when precisely tuned for a specific operating point. However, they lack the flexibility and robustness required to handle dynamic or variable load conditions effectively.

Table 4.3: Scores for each configuration for a fixed load of 100%

Conf #	Devices	Efficiency	Stoichiometry	Minimum flow stack	Stack in pressure	Humidity wrt coolant inlet	Stack in temperature	Weighted score
1	Pressure regulator Liquid ring pump	97.21	100.0	100.0	99.7	95.5	97.7	98.35
2	Pressure regulator Blower	98.12	100.0	100.0	99.7	93.6	96.7	98.40
3	Pressure regulator Ejector							-
4	Pressure regulator Ejector blower hybrid							-
5	Proportional valve Liquid ring pump	97.42	100.0	100.0	100.0	94.8	97.2	98.37
6	Proportional valve Blower	98.28	100.0	100.0	100.0	91.9	96.0	98.29
7	Proportional valve Ejector	98.46	100.0	100.0	100.0	64.8	87.6	95.01
8	Proportional valve Ejector blower hybrid	98.46	100.0	100.0	100.0	64.8	87.6	95.01
9	Mass flow controller Liquid ring pump	96.39	100.0	100.0	2.4	96.1	98.6	81.16
10	Mass flow controller Blower	97.46	100.0	100.0	2.4	96.5	98.3	81.55
11	Mass flow controller Ejector	99.02	100.0	100.0	55.2	52.3	84.1	85.85
12	Mass flow controller Ejector blower hybrid	99.02	100.0	100.0	55.2	52.3	84.1	85.85

Table 4.4: Scores for each configuration for a fixed load of 75%

Conf #	Devices	Efficiency	Stoichiometry	Minimum flow stack	Stack in pressure	Humidity wrt coolant inlet	Stack in temperature	Weighted score
1	Pressure regulator Liquid ring pump	96.83	100.0	100.0	98.6	94.0	97.1	97.83
2	Pressure regulator Blower	97.54	100.0	100.0	98.6	92.4	96.3	97.86
3	Pressure regulator Ejector	98.66	100.0	100.0	57.7	80.0	91.8	89.51
4	Pressure regulator Ejector blower hybrid	98.66	100.0	100.0	57.7	80.0	91.8	89.51
5	Proportional valve Liquid ring pump	97.12	99.9	100.0	100.0	92.8	96.5	97.99
6	Proportional valve Blower	97.79	100.0	100.0	100.0	90.3	95.5	97.92
7	Proportional valve Ejector	97.96	100.0	100.0	100.0	86.4	93.7	97.45
8	Proportional valve Ejector blower hybrid	97.96	100.0	100.0	100.0	86.4	93.7	97.45
9	Mass flow controller Liquid ring pump	95.85	100.0	100.0	2.2	95.4	98.4	80.85
10	Mass flow controller Blower	96.69	100.0	100.0	2.2	95.0	97.9	81.07
11	Mass flow controller Ejector	97.70	100.0	100.0	96.9	88.1	94.2	97.03
12	Mass flow controller Ejector blower hybrid	97.70	100.0	100.0	96.9	88.1	94.2	97.03

4.4. Robustness

4.4.1. Pressure robustness

To evaluate how each configuration responds to real-world supply variations, the supply pressure profile measured on the actual vessel was replicated in the simulation. Since the stack inlet pressure is the parameter most directly influenced by changes in supply pressure, it was selected as the primary metric for analysis. These variations in supply pressure can arise from the presence of multiple BoPs connected to a common supply line; as the hydrogen demand from each BoP fluctuates, the shared supply pressure correspondingly changes.

Figure 4.3 shows the stack inlet pressure over time in response to variations in the supply device's inlet pressure. Minor fluctuations are visible and are caused by the purge valve opening every second. Both the mass flow controller and the pressure regulator follow the general trend of the supply pressure, though with a damped response. In contrast, the proportional valve appears to effectively decouple the stack inlet pressure from supply pressure fluctuations.

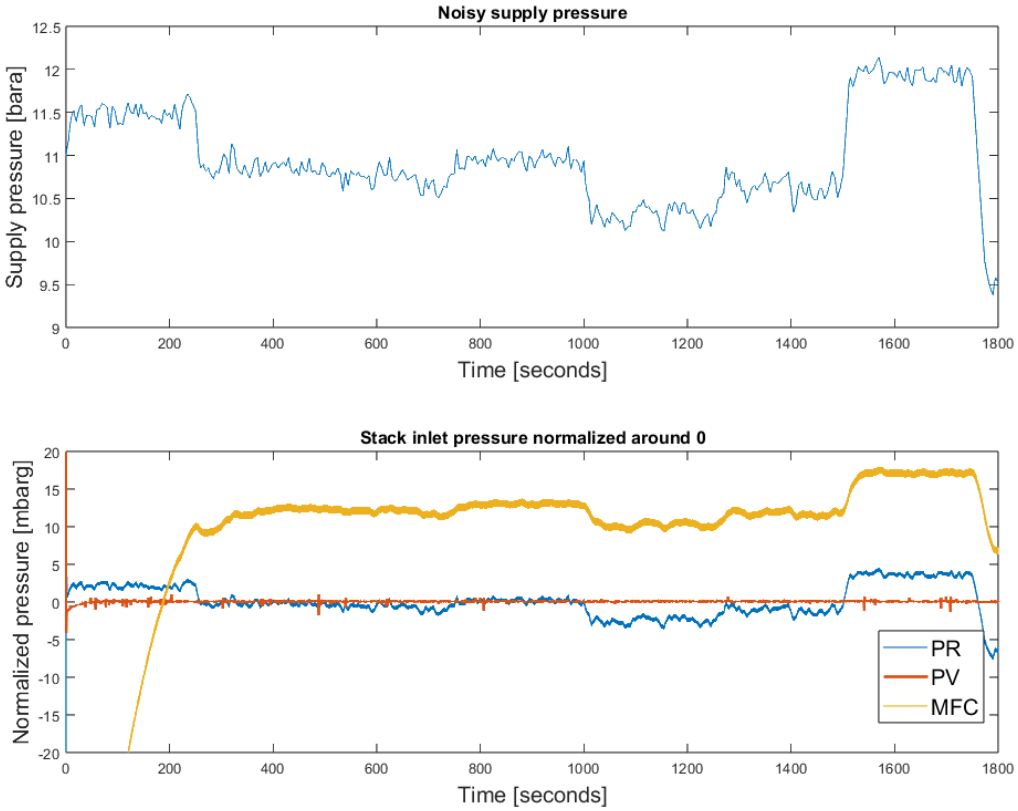

Figure 4.3: Pressure fluctuations caused by fluctuations in supply pressure, inlet pressure is normalized so that the mean is 0

To further investigate the previous findings and quantify their impact, the stack inlet pressure was logged during simulations with supply pressures of 8, 10, and 12 bar. Equations 4.1 and 4.2 were used to get a score, where the mean pressure at different supply pressures is used to get a gradient. The scores can be seen in table 4.5, including the gradient from 8 to 10 bar and 10 to 12 bar. The raw results can be seen in appendix G.

$$\frac{dP}{dt} = \frac{\overline{p}_{12} - \overline{p}_{8}}{12 - 8} \tag{4.1}$$

$$\text{Score} = 100 - \left|\frac{dP}{dt}\right| \tag{4.2}$$

Analysis of supply pressure robustness revealed that pressure regulators and mass flow controllers were more sensitive to inlet pressure fluctuations, whereas proportional valves were able to maintain relatively stable outlet pressures. These findings indicate that proportional valves are preferable for systems requiring high resilience to supply pressure variations. This could be the case when multiple BoP's are connected to the same supply line. When only one BoP is active, the supply pressure will be quite high. When more are activated, the supply pressure will drop, but the system still needs to be able to operate effectively.

Table 4.5: Pressure gradient for each configuration and its pressure robustness score

		Pressure gradient [mbar/bar]			
		8 - 10 bar	8 - 12 bar	10 - 12 bar	Score
1	Pressure regulator Liquid ring pump	3.54	3.11	2.69	96.9
2	Pressure regulator Blower	3.54	3.11	2.69	96.9
3	Pressure regulator Ejector	-	-	-	-
4	Pressure regulator Ejector blower hybrid	-	-	-	-
5	Proportional valve Liquid ring pump	0.00	0.00	0.00	100.0
6	Proportional valve Blower	0.00	0.00	0.00	100.0
7	Proportional valve Ejector	0.10	0.05	-0.01	100.0
8	Proportional valve Ejector blower hybrid	0.03	0.02	0.01	100.0
9	Mass flow controller Liquid ring pump	2.97	2.50	2.03	97.5
10	Mass flow controller Blower	2.92	2.46	2.01	97.5
11	Mass flow controller Ejector	1.42	1.04	0.66	99.0
12	Mass flow controller Ejector blower hybrid	1.64	1.19	0.74	98.8

To say more about the pressure control each supply device has, a simple scenario with an increasing load was simulated, this test the pressure control under increasing supply flow. The pressure traces can be seen in figure 4.4. The proportional valve successfully maintains a constant inlet pressure across the entire load range, demonstrating strong pressure control capabilities. In contrast, the pressure regulator exhibits a significant drop in pressure as the load increases, consistent with the characteristic droop behavior described in section 2.7.1. The mass flow controller initially shows a pressure rise as the loop heats up and water vapor is added. However, instead of stabilizing, the pressure continues to drift upward over time, indicating insufficient long-term control.

When this behavior is evaluated alongside the findings from the pressure robustness analysis, it becomes evident that fluctuating supply pressures, especially under variable load conditions, introduce substantial control challenges. Components with limited adaptability, such as pressure regulators and mass flow controllers, may struggle to maintain stable operating conditions, which can lead to suboptimal system performance and increased risk of stack degradation.

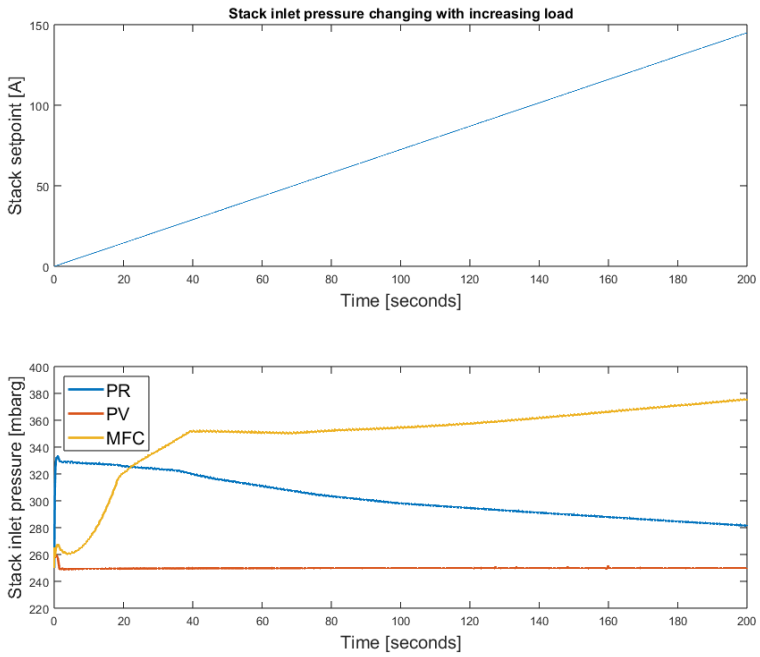

Figure 4.4: The stack inlet pressure (bottom) for each supply device with an increasing stack setpoint (top)

4.4.2. Temperature robustness

Temperature robustness was tested by changing the ambient and supply temperature to correspond with a hot or cold day and comparing that to a normal baseline. Scoring this is done by using equations 4.3, 4.4 and 4.5, all the scores can be seen in table 4.6.

$$\Delta\text{hot score} = \text{normal score} - \text{hot score} \tag{4.3}$$

$$\Delta\text{cold score} = \text{normal score} - \text{cold score} \tag{4.4}$$

$$\text{temperature robustness score} = 100 - \frac{100 \times max(\text{hot score}, \text{cold score})}{\text{normal score}} \tag{4.5}$$

This shows that temperature robustness is relatively consistent across all configurations, though systems incorporating an ejector exhibit slightly greater sensitivity. This is primarily due to their lower hydrogen stoichiometry at higher setpoints compared to configurations using pumps (see figure 4.2). As a result, ejector-based systems are more affected by changes in temperature. Additionally, elevated temperatures lead to an increased entrainment ratio in ejectors, which alters the recirculation behavior. In contrast, for pump-based systems, higher temperatures cause an increase in pressure drop across the stack. This triggers the pump to reduce its speed setpoint as it is controlled on pressure drop over the stack, which in turn mitigates the impact of the temperature rise, effectively dampening the temperature gain. The main parameters influenced by temperature changes are relative humidity and the gas temperature itself. As temperature increases, the hydrogen stream can hold more water vapor, thereby improving humidification. In the case of this system, both humidity and temperature are below optimal levels under standard conditions. Therefore, raising the supply and ambient temperatures will enhance performance. However, this effect may not generalize to all PEM fuel cell BoP systems, as optimal conditions depend on specific design and operating parameters.

Table 4.6: Temperature robustness score for each configuration

		Δhot score	Δcold score	Score
1	Pressure regulator Liquid ring pump	0.61	1.63	98.3
2	Pressure regulator Blower	0.66	1.72	98.2
3	Pressure regulator Ejector	-	-	-
4	Pressure regulator Ejector blower hybrid	-	-	-
5	Proportional valve Liquid ring pump	0.65	1.73	98.2
6	Proportional valve Blower	0.71	1.80	98.2
7	Proportional valve Ejector	2.06	3.31	96.4
8	Proportional valve Ejector blower hybrid	1.30	2.29	97.6
9	Mass flow controller Liquid ring pump	0.59	1.16	98.6
10	Mass flow controller Blower	2.13	1.21	97.4
11	Mass flow controller Ejector	3.37	4.78	93.9
12	Mass flow controller Ejector blower hybrid	2.41	3.59	95.8

4.4.3. Water crossover

Variation in water crossover rates between 20%, 25%, and 30% exhibited a negligible impact on performance. Nevertheless, significant increases in water crossover (above 50%) could substantially affect pressure drops, condensation behavior, and the operational integrity of pumps or ejectors, which are effects that were not captured in the current model.

4.4.4. Stoichiometry

Lastly, it was observed that operating at higher stoichiometry generally improved configuration scores by enhancing recirculation and thereby increasing stack inlet temperature and humidity, this would outweigh the extra power needed for recirculation. A maximum would be reached when all scores would reach 100, this would be around a stoichiometry of 2.1. The liquid ring pump used for this model was not able to reach this stoichiometry at the higher setpoint, so this was not further investigated, as this would make comparisons unfair. Furthermore, increasing the stoichiometry of the ejector is not possible without changing its geometry.

4.5. Transient load

To assess the transient behavior of each configuration, a dynamic load profile was applied, both with and without a rate limiter. The rate limiter used was based on specifications provided by the stack manufacturer. The applied load profile is shown in figure 4.5, and the resulting time-series plots comparing responses with and without the rate limiter are presented in appendix H.

Because quantifying settling time proved unreliable across configurations, the analysis focused on qualitative evaluation of the transient responses shown in the plots. These revealed subtle but important differences in system dynamics. Configurations using pumps generally responded quickly, with performance primarily constrained by the rate limiter. An exception was observed in the mass flow controller setup, where the stack inlet pressure did not consistently reach a steady state. In contrast, configurations using an ejector or hybrid recirculation device exhibited more pronounced oscillations, particularly

in the absence of a rate limiter, indicating greater sensitivity to load transients. Interestingly, when the mass flow controller was paired with either an ejector or hybrid system, a steady-state pressure was achieved, and this occurred more rapidly when a rate limiter was applied.

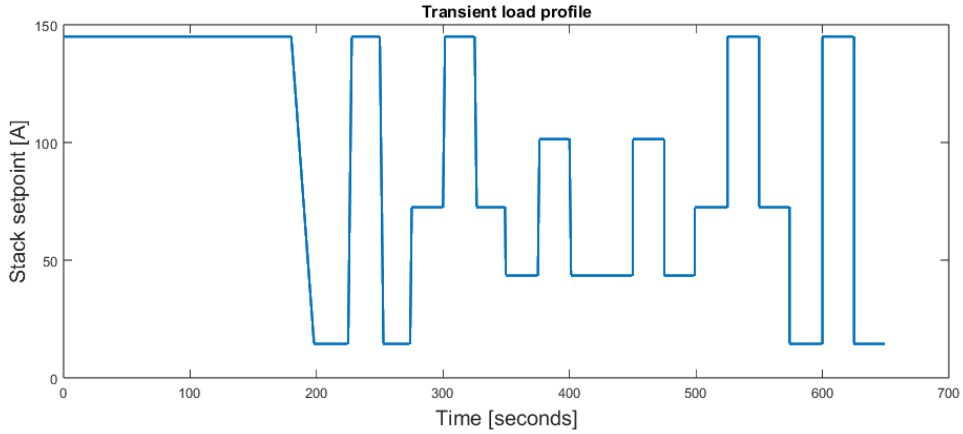

Figure 4.5: Dynamic load profile used to assess transient system responses with and without rate limiter

4.6. Combined scores

For easy comparison, table 4.7 groups all the scores. For getting an overall score, the scores are multiplied to more clearly show differences between configurations. In figure 4.6, one can see the multiplied scores of each configuration. The combined performance scores demonstrated that configurations utilizing a proportional valve in combination with either a blower or a liquid ring pump achieved the highest results. They edge out the rest of the top five on their higher pressure robustness and ability to run at higher stoichiometry over the whole range compared to the best placed ejector configuration. The combination of a pressure regulator with an ejector or hybrid score very low because of their limited working range. Any configuration with a mass flow controller scores low because it has no direct control over the pressure in the loop and is less robust compared to others.

Table 4.7: Summary table showing the combined performance, robustness, and operating range scores of each configuration

Conf #	Devices	Load sweep	100% load score	75% load score	Robustness pressure score	Robustness temperature score	Range	Multiplied score
1	Pressure regulator Liquid ring pump	97.01	98.3	97.8	96.9	98.3	100.0	88.9
2	Pressure regulator Blower	97.17	98.4	97.9	96.9	98.2	100.0	89.1
3	Pressure regulator Ejector	-	-	89.5	-	-	8.3	7.4
4	Pressure regulator Ejector blower hybrid	-	-	89.5	-	-	6.9	6.2
5	Proportional valve Liquid ring pump	97.94	98.4	98.0	100.0	98.2	100.0	92.7
6	Proportional valve Blower	98.02	98.3	97.9	100.0	98.2	100.0	92.6
7	Proportional valve Ejector	91.97	95.0	97.5	100.0	96.4	69.7	57.2
8	Proportional valve Ejector blower hybrid	97.41	95.0	97.5	100.0	97.6	100.0	88.1
9	Mass flow controller Liquid ring pump	80.67	81.2	80.9	97.5	98.6	100.0	50.9
10	Mass flow controller Blower	80.96	81.6	81.1	97.5	97.4	100.0	50.8
11	Mass flow controller Ejector	77.99	85.9	97.0	99.0	93.9	60.0	36.2
12	Mass flow controller Ejector blower hybrid	85.50	85.9	97.0	98.8	95.8	60.0	40.5

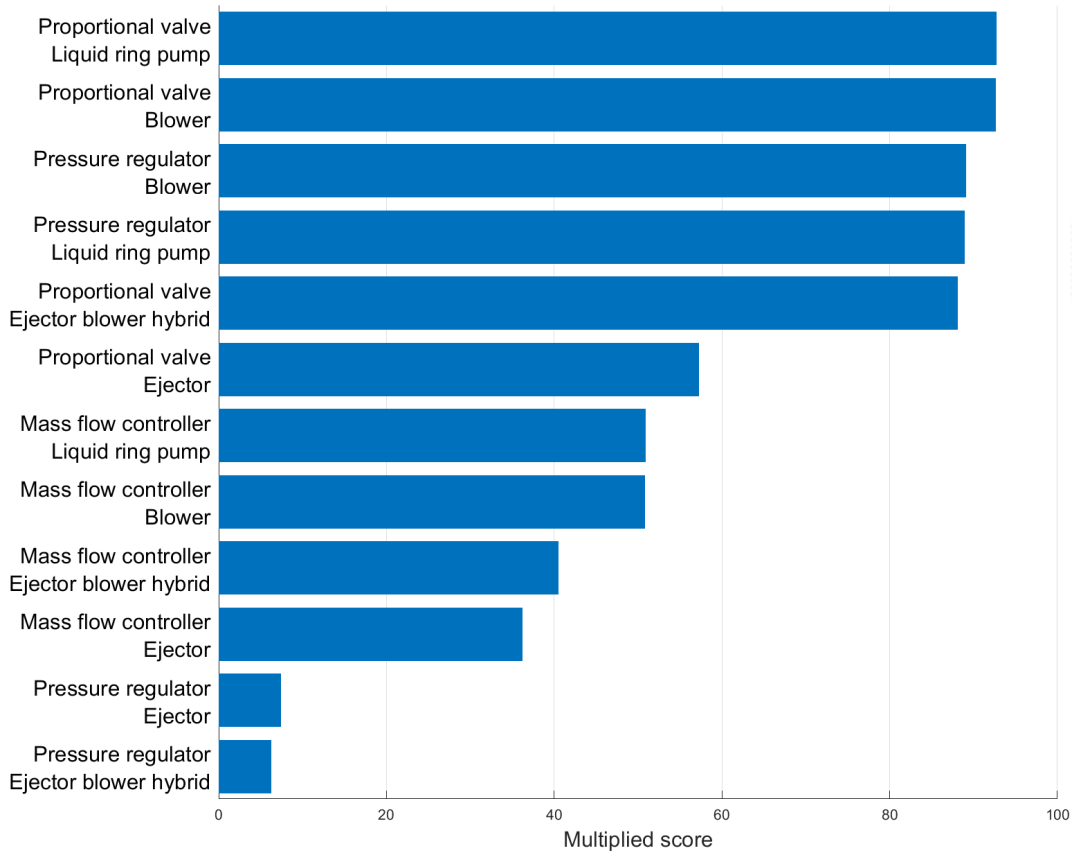

Figure 4.6: Multiplied scores of all configurations, ranked from highest to lowest, to visually compare overall performance

4.7. Relationships between system parameters

Five key parameters are monitored in this study: temperature, relative humidity, flow, stoichiometry, and pressure. Figure 4.7 illustrates how these variables are interconnected within the hydrogen loop.

Temperature and relative humidity are primarily influenced by the ratio between recirculated and supply flow. Since the recirculated stream is typically warmer and more humid than the fresh supply, increasing the recirculation flow raises both temperature and humidity levels in the system. This same flow ratio also affects stoichiometry, which reflects the amount of excess hydrogen delivered relative to what is consumed by the stack. Because the recirculation flow is governed by the recirculation device, and it indirectly influences both temperature and humidity, these two parameters can serve as useful indicators of recirculation behavior.

In contrast, the supply flow is determined by the stack setpoint, as the supply device attempts to match the hydrogen consumption rate. If this balance is not maintained, system pressure will deviate, either increasing or decreasing, making pressure a direct outcome of the supply control strategy.

While this conceptual framework simplifies the system by omitting purge losses and minor leakages, their overall influence is relatively small and does not significantly alter the observed trends. In ejector-based systems, however, these relationships become more complex. Because the ejector directly couples recirculated flow to supply flow, the system becomes heavily dependent on the stack setpoint and the ejector geometry, reducing the degree of independent control over parameters such as stoichiometry, pressure, and humidity.

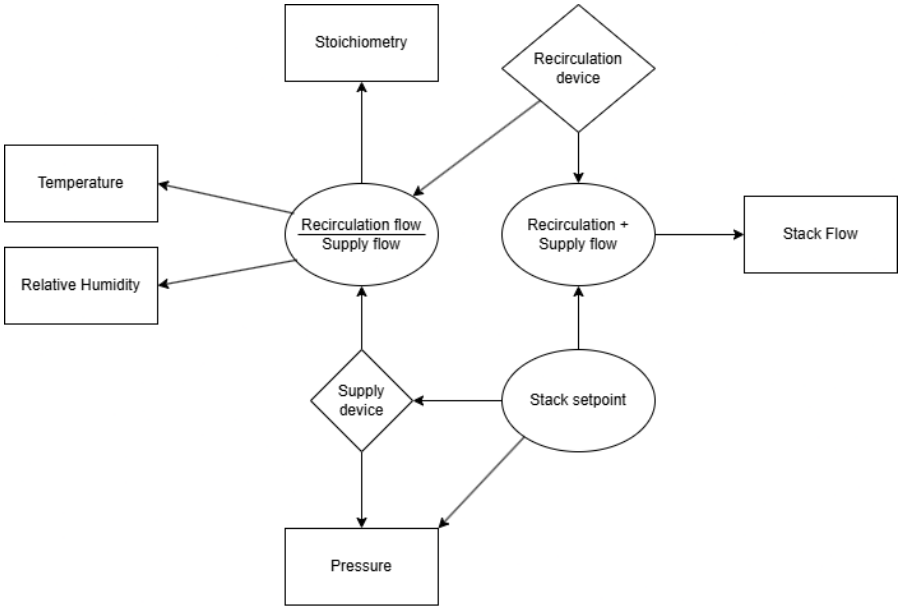

Figure 4.7: Schematic showing how supply and recirculation components influence key system parameters.

Box plots of these five parameters across all component configurations, supporting the relationships, can be seen in appendix I. It becomes clear that the pressure score is dependent on the supply device. This also shows that a mass flow controller is an inferior supply device as its pressure score is generally low. For the recirculation device, all of them are able to reach the minimum flow target, but the blower and pump have better control over it and can easily increase or decrease the stoichiometry and thus affecting temperature and relative humidity. For an ejector, the recirculation rate is fixed, thus allows minimal control.

4.8. Evaluation of configuration attributes

In this section, the inherent attributes of each configuration are evaluated independently of their performance. A comparative analysis was conducted by comparing component complexity, control complexity, flexibility, reliability, availability, and maintainability. Each device was qualitatively scored on a scale from 1 (low) to 5 (high), based on design characteristics, control requirements, and operational behavior within the system context.
Component complexity refers to the number of physical parts required, including supporting hardware. A score of 5 was given to single-component solutions, with one point deducted for each additional required component. The liquid ring pump scored the lowest due to its need for a pump, motor, motor controller, and liquid piping. The blower scored slightly better due to its simpler integration. Both the ejector and pressure regulator received the highest score, as they operate with only one component. Proportional valves and mass flow controllers require an additional sensor, reducing their scores. Control complexity reflects the number and difficulty of control loops involved. The pressure regulator does not require a control loop, hence, it scores highest. The mass flow controller uses a closed-loop system, usually pre-tuned by the manufacturer. The ejector requires purge control when operating outside of its design range.

Flexibility refers to the device's ability to influence key system parameters. Both the liquid ring pump and blower offer high flexibility through direct control of the recirculation flow, allowing the ability to increase stoichiometry. The proportional valve allows a tunable outlet pressure. The ejector is limited in flexibility but can be enhanced through techniques such as pulsing or additional purging. Reliability and availability assess long-term dependability and uptime. Passive components like the ejector score highest, as they have no moving parts. Maintainability evaluates how easy it is to service or repair a device, including expected downtime. Devices with more complex or moving parts, such as the liquid ring pump, generally score lower in this category. The scoring results are shown in table 4.8.

Table 4.8: Qualitative scores (1 = low, 5 = high) for system-level attributes of hydrogen loop components. Low scores are highlighted in red.

Devices	Component Complexity	Control Complexity	Flexibility	Reliability	Availability	Maintainability
Pressure regulator	5	5	1	4	4	4
Proportional valve	4	3	4	3	4	3
Mass flow controller	4	4	3	3	3	3
Liquid ring pump	2	3	5	3	3	2
Blower	3	3	4	4	4	4
Ejector	5	4	2	5	5	5
Hybrid	2	3	4	4	4	3

Table 4.9 aggregates these scores by configuration. The total score for each criterion is the sum of both included devices, giving values from 2 to 10. Notably, configurations 3 and 4 score very high in most system-level categories. However, based on earlier performance analysis, it is not considered a suitable option, showing that high system-level robustness does not always correlate with performance.

Table 4.9: Aggregate system-level scores (2 = low, 10 = high) for each configuration based on combined component attributes. Low scores are highlighted in red.

Conf #	Devices	Component Complexity	Control Complexity	Flexibility	Reliability	Availability	Maintainability
1	Pressure regulator Liquid ring pump	7	8	6	7	7	6
2	Pressure regulator Blower	8	8	5	8	8	8
3	Pressure regulator Ejector	10	9	3	9	9	9
4	Pressure regulator Ejector blower hybrid	7	8	5	8	8	7
5	Proportional valve Liquid ring pump	6	6	9	6	7	5
6	Proportional valve Blower	7	6	8	7	8	7
7	Proportional valve Ejector	9	7	6	8	9	8
8	Proportional valve Ejector blower hybrid	6	6	8	7	8	6
9	Mass flow controller Liquid ring pump	6	7	8	6	6	5
10	Mass flow controller Blower	7	7	7	7	7	7
11	Mass flow controller Ejector	9	8	5	8	8	8
12	Mass flow controller Ejector blower hybrid	6	7	7	7	7	6

4.9. Assumptions

Several assumptions were made in the development of the model, which are important to consider when interpreting the results. Among the most significant are the flow curves used for the pressure regulator, liquid ring pump, and blower. While these curves are representative of typical performance for each device type, using alternatives from different manufacturers could result in different system behavior and overall outcomes. The performance curve for the ejector was calculated under the assumption that no liquid water would be present in the flow. In reality, liquid water is present and if significant, can cause lower ejector performance.

All PID controllers in the model assume perfect sensing, without accounting for sensor noise or signal delay. In practice, these imperfections can degrade system performance, particularly in scenarios

involving robustness and transient response.

The fuel cell stack is modeled as a simplified hydrogen consumer with high thermal inertia, resulting in a constant outlet temperature. In real applications, stack temperature varies based on factors such as cooling strategy and air supply, and warm-up behavior is not captured in the current model. Additionally, evaporation and condensation within the stack are not modeled, which may influence humidity dynamics and transient thermal behavior. The model and corresponding results are based on a fuel cell operating at a fixed anode pressure. For systems that operate under variable pressure conditions, the findings may differ. Most notably, a pressure regulator would no longer be a viable solution due to its inability to adjust the outlet pressure dynamically.

The air supply system can significantly affect hydrogen loop behavior, especially during ramp-up/ramp-down phases, as well as influencing nitrogen and water crossover. As discussed in paragraph 4.4.3, small variations in water crossover were found to have minimal impact on system behavior. Nitrogen crossover was neglected altogether, but it could be incorporated into the model if accurate data and parameters for a specific stack are available. In this study, the system was predominantly temperature- and humidity-limited, meaning those parameters were generally below or near their targets, but never exceeded. As a result, increased recirculation was always beneficial.

5

Conclusion

This study conducted a detailed evaluation of twelve different hydrogen loop configurations for maritime PEM fuel cell applications. Each configuration combined different supply and recirculation components, including a pressure regulator, proportional valve, mass flow controller, liquid ring pump, blower, ejector, and ejector-blower hybrid. They were assessed based on multiple criteria, including efficiency, performance, robustness to dynamic and environmental changes, and overall system attributes. By modeling these configurations under realistic maritime operating conditions, valuable insights were obtained into the relative advantages and limitations of each approach. The modeling framework developed in this work sets itself apart through its dynamic approach that enables comparative scoring under realistic maritime conditions, a novel contribution to hydrogen BoP design methodology.

A key observation is that while ejector-based systems offer the theoretical advantage of no recirculation power consumption, this efficiency gain is practically negligible in maritime applications. The power saved in recirculation is relatively small compared to the total output power of the fuel cell stack. Moreover, ejectors suffer from limitations at low load operating points, where sufficient primary flow is not available for proper recirculation. This can lead to operational risks, such as flooding unless more complex ejector-blower hybrid systems are employed. In real-world maritime settings, ships often deploy multiple BoPs to meet higher power demands. This opens the possibility of using ejectors selectively: employing ejector-based recirculation for systems operating mainly at high loads, while equipping at least one system with an active recirculation device (such as a blower or pump) to ensure reliable operation during low-load scenarios. This hybrid deployment could optimize overall efficiency without compromising system robustness.

Additionally, a deeper understanding was developed of the complex interrelationships between system parameters such as temperature, relative humidity, stoichiometry, and pressure. The ratio between recirculated and supply flow was identified as a central factor influencing both temperature and humidity levels, which in turn affect overall stack performance. Supply flow is primarily driven by the stack setpoint, and any imbalance directly affects system pressure. These interdependencies emphasize the need for supply and recirculation systems that can finely control flows to maintain optimal operating conditions, particularly under dynamic maritime conditions.

Among the configurations studied, the proportional valve–liquid ring pump configurations delivered the highest performance scores. However, when considering practical factors such as system complexity, power consumption, reliability, and maintainability, the proportional valve–blower configuration emerges as the recommended solution. Although it achieved marginally lower performance scores, it significantly outperforms the liquid ring pump system in terms of simplicity, reliability, and ease of maintenance, critical factors for maritime operations where robustness and serviceability are paramount. This conclusion is based on the assumption that only the hydrogen loop components are varied, while all other parts of the Balance of Plant are held constant or excluded from analysis. Therefore, it reflects the optimal choice within the defined scope and modeling assumptions of this study.

In conclusion, for maritime PEM fuel cell BoP systems, a supply system based on a proportional valve-blower configuration is the best compromise between performance, operational flexibility, efficiency, and long-term reliability. While ejectors remain attractive for specific high-load applications, active recirculation systems provide the necessary versatility to support real-world operating conditions across all load regimes. This research can support future BoP designs by enabling more informed decision-making. By simulating a wide range of dynamic scenarios and practical component configurations, the findings contribute to bridging the gap between theoretical system design and scalable, robust implementations suitable for the evolving demands of the maritime energy transition.

5.1. Key takeaways per configuration type

Based on the results of this study, some clear patterns emerged about how different components behave and perform. This section gives a brief summary of the main findings for each type of supply and recirculation device, as well as the overall best-performing setup. The goal is to give a straightforward overview that can help guide future design choices when putting together a hydrogen loop for PEM fuel cell systems.

- **Supply components**
  - **Pressure regulator**: Robust and passive, but not adjustable during operation.
  - **Proportional valve**: Offers the best dynamic control but requires careful tuning.
  - **Mass flow controller**: Simplifies control architecture, but lacks pressure regulation.
- **Recirculation components**
  - **Liquid ring pump**: Achieves the highest temperature and humidity, but is complex and consumes significant power.
  - **Blower**: Mechanically simple and offers good operational flexibility.
  - **Ejector**: No moving parts and no power consumption, but suffers from limited controllability and operational range.
  - **Ejector-blower hybrid**: Combines the efficiency of ejectors with the low-load flexibility of blowers, at the cost of increased complexity and control effort.
- **Best overall configuration**
  - **Proportional valve + blower**: Most balanced setup, offering a wide working range, high efficiency, and manageable complexity.

6

Further Research

While this thesis has presented a comprehensive simulation-based evaluation of twelve hydrogen loop configurations for maritime PEM fuel cell systems, several opportunities exist for expanding and deepening the research.

One logical extension is the inclusion of a broader set of component options. Additional supply and recirculation devices, such as hydrogen injectors, scroll and screw compressors, and electrochemical pumps, could introduce different performance characteristics. Similarly, repeating the analysis using equivalent components from various manufacturers would allow for benchmarking and increase the robustness and applicability of the findings. The ejector used in this study was deliberately sized to cover a broad operating range. However, differently sized ejectors optimized for specific load segments may deliver improved efficiency or responsiveness.

A similar targeted approach could be applied to other BoP components, like air supply or cooling, to further refine configuration selection for those systems. Furthermore, humidifiers and heaters were not included in the model under the assumption that they were unnecessary; future work could test this assumption by incorporating these components and assessing their impact.

Several important subsystems and physical phenomena were excluded from this study, yet they have the potential to significantly affect hydrogen loop performance, control strategies, and overall system behavior. These include nitrogen crossover, the air supply system, and the cooling system. In addition, the absence of a detailed fuel cell voltage model limits the ability to directly link loop performance to electrical efficiency.

Nitrogen crossover occurs when nitrogen from the cathode side diffuses through the membrane into the anode. This increases the pressure drop in the system and alters the anode gas composition. Accurately modeling this phenomenon would allow for a more realistic representation of anode-side conditions and enable optimization of the purge strategy.

Although not explicitly modeled, the air supply system can also influence hydrogen loop behavior. Cathode-side parameters affect both nitrogen and water crossover, while the air flow rate and temperature can impact overall stack temperature and, consequently, the thermal conditions on the hydrogen loop side. Similarly, the cooling system, also not included in the current model, plays a critical role in managing the thermal behavior of the BoP and directly affects gas properties within the hydrogen loop.

Finally, this study does not incorporate a detailed stack voltage model that accounts for the effects of temperature, pressure, and humidity on fuel cell voltage. Including such a model would enable direct evaluation of electrical performance and efficiency, providing another metric for comparing configurations. Future work could benefit from integrating these omitted subsystems and physical effects to enhance model accuracy and practical relevance.

To support long-term system optimization, the simulation model could be integrated with fuel cell degradation models. This would provide insight into how various configurations impact system durability over time. In parallel, including cost, maintenance frequency, and reliability data would enable lifecycle-based evaluation and support practical system design decisions.

Experimental data can enhance both the validity of the model and the reliability of the results presented in this thesis. An ideal test setup would allow for easy swapping of components and enable consistent testing across different devices. Such a setup would not only support model validation but also generate valuable standalone data, helping to identify control limitations and assess dynamic performance under transient conditions.

Lastly, while this work has focused on maritime fuel cell systems, the same modeling framework can be adapted to other application sectors. Sectors such as heavy-duty transport, stationary power generation, and automotive fuel cells have distinct performance priorities and constraints. Applying this methodology to those contexts could help identify optimized hydrogen loop configurations tailored to their specific demands. Furthermore, this model could be used to test and compare different control strategies or procedures, like start-up and shutdown. Several adjustments might need to be made to the model for this.

In summary, extending this research across components, subsystems, operational domains, and real-world validation will provide a more holistic understanding of hydrogen loop design and guide the deployment of robust, efficient fuel cell systems across a wide range of applications.

Additionally, this research was conducted using a specific fuel cell stack, and the model can be adapted for stacks with different operational characteristics. A key feature of the stack used in this study is that it operates at a fixed anode pressure, regardless of power setpoint. In contrast, many other stacks increase their operating pressure with increasing load. If such a stack were used, a pressure regulator would no longer be a viable supply device, as its fixed outlet pressure would be incompatible with the dynamic pressure requirements of the stack.

Bibliography

[1] *Future Proof Shipping – Creating a zero-emissions shipping world*. URL: https://futureproofshipping.com/.

[2] S. Toghyani, E. Afshari, and E. Baniasadi. “A parametric comparison of three fuel recirculation system in the closed loop fuel supply system of PEM fuel cell”. In: *International journal of hydrogen energy* 44.14 (Mar. 2019), pp. 7518–7530. ISSN: 03603199. DOI: 10.1016/j.ijhydene.2019.01.260.

[3] Yuanyang Zhao et al. “Air and hydrogen supply systems and equipment for PEM fuel cells: a review”. In: *International Journal of Green Energy* 19.4 (Sept. 21, 2021), pp. 331–348. DOI: 10.1080/15435075.2021.1946812.

[4] Kun-Yang Shen, Suhan Park, and Young-Bae Kim. “Hydrogen utilization enhancement of proton exchange membrane fuel cell with anode recirculation system through a purge strategy”. In: *International journal of hydrogen energy* 45.33 (June 2020), pp. 16773–16786. ISSN: 03603199. DOI: 10.1016/j.ijhydene.2020.04.147.

[5] Paul Rodatz et al. “EFFICIENCY IMPROVEMENTS BY PULSED HYDROGEN SUPPLY IN PEM FUEL CELL SYSTEMS”. In: *IFAC Proceedings Volumes* 35.1 (Jan. 2002), pp. 259–264. DOI: 10.3182/20020721-6-es-1901.01511.

[6] B. Wu, M. Matian, and G. J. Offer. “Hydrogen PEMFC system for automotive applications”. In: *International Journal of Low-Carbon Technologies* 7.1 (Mar. 2012), pp. 28–37. ISSN: 1748-1317. DOI: 10.1093/ijlct/ctr026.

[7] Qingqing Zhang et al. “3D transient CFD modelling of a scroll-type hydrogen pump used in FCVs”. In: *International journal of hydrogen energy* 43.41 (Oct. 2018), pp. 19231–19241. ISSN: 03603199. DOI: 10.1016/j.ijhydene.2018.08.158.

[8] M. Badami and M. Mura. “Theoretical model with experimental validation of a regenerative blower for hydrogen recirculation in a PEM fuel cell system”. In: *Energy Conversion and Management* 51.3 (Mar. 2010), pp. 553–560. ISSN: 01968904. DOI: 10.1016/j.enconman.2009.10.022.

[9] Jixin Chen et al. “Modeling a hydrogen pressure regulator in a fuel cell system with Joule–Thomson effect”. In: *International journal of hydrogen energy* 44.2 (Jan. 2019), pp. 1272–1287. ISSN: 03603199. DOI: 10.1016/j.ijhydene.2018.11.020.

[10] Muhammad Ramzan and Adnan Maqsood. “Dynamic modeling and analysis of a high pressure regulator”. In: *Mathematical Problems in Engineering* 2016 (2016), pp. 1–8. ISSN: 1024-123X. DOI: 10.1155/2016/1307181.

[11] Si Huang et al. “Theoretical model for the performance of liquid ring pump based on the actual operating cycle”. In: *International Journal of Rotating Machinery* 2017 (2017), pp. 1–9. ISSN: 1023-621X. DOI: 10.1155/2017/3617321.

[12] Department of Hydrodynamic Systems Fluid Machinery and András Szabó. *Measurement of a liquid ring vacuum pump*. Tech. rep. Apr. 2021. URL: https://www.hds.bme.hu/letoltesek/targyak/BMEGEVGBX01_ENG/Vi_eng_v2.pdf.

[13] M. ELSayed Youssef, Khairia E. AL-NAdi, and Moataz H. Khalil. “Lumped model for proton exchange membrane fuel cell (PEMFC)”. In: *International Journal of Electrochemical Science* 5.2 (Feb. 2010), pp. 267–277. ISSN: 14523981. DOI: 10.1016/S1452-3981(23)15283-7.

[14] Gyu-Yeong Choe et al. “Proton exchange membrane fuel cell (PEMFC) modeling for high efficiency fuel cell balance of plant (BOP)”. In: *2007 International Conference on Electrical Machines and Systems (ICEMS)*. IEEE, Oct. 2007, pp. 271–276. DOI: 10.1109/{ICEMS12746}.2007.4412239.

[15] Xiaochen Yu, Biao Zhou, and Andrzej Sobiesiak. “Water and thermal management for Ballard PEM fuel cell stack”. In: *Journal of Power Sources* 147.1-2 (Mar. 11, 2005), pp. 184–195. DOI: 10.1016/j.jpowsour.2005.01.030.

[16] James Larminie and Andrew Dicks. *Fuel cell systems explained*. Wiley-Blackwell, Mar. 28, 2003.

[17] Frano Barbir. *PEM fuel cells. Theory and Practice*. Academic Press, Sept. 25, 2012.

[18] Nedstack Fuel Cell Technology. *PRODUCT DATA SHEET FCS 13-XXL Gen 2.9*. Tech. rep. May 2022. URL: https://nedstack.com/sites/default/files/2022-07/nedstack-fcs-13-xxl-gen-2.9-datasheet-rev01.pdf.

[19] *Fuel cell stacks | EKPO Fuel Cell Technologies*. URL: https://www.ekpo-fuelcell.com/en/products-technology/fuel-cell-stacks.

[20] *How does a Direct-Operated Pressure Regulator work? (Part 2)*. Oct. 6, 2022. URL: https://emersonexchange365.com/products/valves-actuators-regulators/f/actuators-regulators-other-final-control/6264/how-does-a-direct-operated-pressure-regulator-work-part-2.

[21] *Pressure Regulator Flow Curves. Technical Bulletin*. URL: https://www.swagelok.com/downloads/webcatalogs/en/ms-06-114.pdf (visited on 11/11/2024).

[22] SMLease. *What is Solenoid Valve and How does a Solenoid Valve Work?* June 4, 2021. URL: https://www.smlease.com/entries/automation/what-is-solenoid-valve-and-how-does-solenoid-valves-work/.

[23] Doug Robertson. *Gas Mass Flow Controllers - An Overview of Technologies | Clippard Knowledgebase*. URL: https://www.clippard.com/cms/wiki/gas-mass-flow-controllers-overview-technologies.

[24] Gerald Singer et al. “A development toolchain for a pulsed injector-ejector unit for PEM fuel cell applications”. In: *International Journal of Hydrogen Energy* 47.56 (June 15, 2022), pp. 23818–23832. DOI: 10.1016/j.ijhydene.2022.05.177.

[25] *Graham Corporation Technical Article: Liquid Ring Vacuum Pump Suction Control*. Nov. 2020. URL: https://myemail.constantcontact.com/Graham-Corporation-Technical-Article--Liquid-Ring-Vacuum-Pump-Suction-Control.html?aid=40cVKPtA-bM&soid=1130222917333&utm_source=chatgpt.com.

[26] *Busch Liquid Ring Vacuum & Overpressure Technology | Busch United States*. URL: https://www.buschvacuum.com/us/en/products/vacuum-pumps/liquid-ring/liquid-ring-technology/.

[27] AirCompressorWorks. *Compressor Basics: Rotary lobe pump*. Nov. 2017. URL: https://aircompressorworks.com/compressor-basics-rotary-lobe-pump.

[28] Ipieca. *Ejectors (2022)*. Nov. 2022. URL: https://www.ipieca.org/resources/energy-efficiency-compendium-online/ejectors-2022.

[29] Bowen Wang, Hao Deng, and Kui Jiao. “Purge strategy optimization of proton exchange membrane fuel cell with anode recirculation”. In: *Applied Energy* 225 (Sept. 2018), pp. 1–13. ISSN: 03062619. DOI: 10.1016/j.apenergy.2018.04.058.

[30] Vern Sproat and Debbie LaHurd. *Fuel Cell Balance-of-Plant Reliability Testbed Project*. Oct. 29, 2016. DOI: 10.2172/1335164.

[31] Shinae Lee, Dao Zhou, and Huai Wang. “Reliablity assessment of fuel cell system - A framework for quantitative approach”. In: *2022 IEEE Energy Conversion Congress and Exposition (ECCE)* 396 (Sept. 1, 2016), pp. 1–5. DOI: 10.1109/ecce.2016.7855391.

[32] Arden L. Buck. “New Equations for Computing Vapor Pressure and Enhancement Factor”. In: *AMETSOC* (Dec. 1981). DOI: 10.1175/1520-0450(1981)020.

[33] *Voir®H2 anode water separator-Voir-H2*. URL: http://h2.voir-tech.com.cn/en/productlist-2-21-1.html.

[34] *Fluid Calculator*. URL: https://www.burkert.com/en/service-support/knowledge-center/glossary/fluid-calculator.

[35] Christian Bürkert GmbH & Co. KG. *PWM control electronics for electromagnetic proportional valves*. Tech. rep. URL: https://www.burkert.com/en/Media/plm/DTS/DS/ds6223-standard-eu-en.pdf.

[36] pdblowers. *www.pdblowers.com*. Tech. rep. URL: https://www.pdblowers.com/wp-content/uploads/2018/11/URAI-24-Blower-Data-Sheet.pdf.

[37] WeiXiong Chen et al. "A 1D model to predict ejector performance at critical and sub-critical operational regimes". In: *International Journal of Refrigeration* 36.6 (Apr. 2013), pp. 1750–1761. DOI: 10.1016/j.ijrefrig.2013.04.009.

[38] Chao Li, Baigang Sun, and Qinghe Luo. "Effect of Structural Parameters and Operational Characteristic Analysis on Ejector Used in Proton Exchange Membrane Fuel Cell". In: *Sustainability* 14.15 (July 2022), p. 9205. DOI: 10.3390/su14159205.

[39] Tao Zhang et al. "Numerical analysis of key structural parameters of ejector for PEMFC system under low power conditions". In: *Vibroengineering PROCEDIA* 44 (Aug. 2022), pp. 117–123. DOI: 10.21595/vp.2022.22700.

[40] Mansu Kim et al. "Effects of anode flooding on the performance degradation of polymer electrolyte membrane fuel cells". In: *Journal of Power Sources* 266 (May 2014), pp. 332–340. DOI: 10.1016/j.jpowsour.2014.04.092.

[41] Anthony Mills and Carlos F. M. Coimbra. *Basic heat transfer*. Temporal Publishing, Aug. 2015.

[42] R.W. Lockhart and R.C. Martinelli. "Proposed correlation of data for isothermal two-phase, two-component flow in pipes". In: *Chemical Engineering Progress* 45.1 (1949), pp. 39–48.

[43] D. Chisholm. "A theoretical basis for the Lockhart-Martinelli correlation for two-phase flow". In: *International Journal of Heat and Mass Transfer* 10.12 (Dec. 1967), pp. 1767–1778. DOI: 10.1016/0017-9310(67)90047-6.

[44] James Welty et al. *Fundamentals of momentum, heat and mass transfer*. Wiley, Nov. 2007.

[45] Arun K. Pal and A. K. Barua. "Viscosity of hydrogen - nitrogen and hydrogen - ammonia gas mixtures". In: *The Journal of Chemical Physics* 47.1 (July 1967), pp. 216–218. ISSN: 0021-9606. DOI: 10.1063/1.1711848.

A

Configurations

This appendix presents the twelve hydrogen loop configurations investigated in this master's thesis using a dynamic MATLAB Simulink model. Each configuration represents a unique combination of supply and recirculation devices. The goal of this study is to evaluate how different device combinations influence system performance, control behavior, and operational robustness under realistic maritime fuel cell conditions.

The configurations are based on a selection of three supply device types, a pressure regulator, a proportional valve, and a mass flow controller, and four recirculation device types, a liquid ring pump, a blower, an ejector, and an ejector–blower hybrid. These devices were chosen not only because they represent a broad range of control strategies, mechanical complexity, and energy efficiency characteristics, but also because they are among the most commonly used solutions in PEM fuel cell systems.

Table A.1: All twelve configurations to be examined

Configuration	Supply device	Recirculation device
1	Pressure regulator	Liquid ring pump
2	Pressure regulator	Blower
3	Pressure regulator	Ejector
4	Pressure regulator	Ejector blower hybrid
5	Proportional valve	Liquid ring pump
6	Proportional valve	Blower
7	Proportional valve	Ejector
8	Proportional valve	Ejector blower hybrid
9	Mass flow controller	Liquid ring pump
10	Mass flow controller	Blower
11	Mass flow controller	Ejector
12	Mass flow controller	Ejector blower hybrid

B

Model Overview

Figures B.1 and B.2 show the MATLAB Simulink models used for simulating the hydrogen loop configurations. Separate models were developed for pump-based and ejector-based systems to accurately reflect differences in component placement and flow paths in the physical system. In these diagrams, each color represents a specific function or component type within the system:

- Yellow blocks indicate system volumes,
- Blue blocks represent flow resistances between volumes,
- Pink denotes the supply device,
- Green marks the recirculation device,
- Red corresponds to the controller for the recirculation device,
- Orange indicates the water separator, whose placement varies depending on the configuration,
- White is used for the purge valve and pressure relief valve and for the ejector in figure B.2,
- Cyan represents the fuel cell stack controller, which provides the stack setpoint.

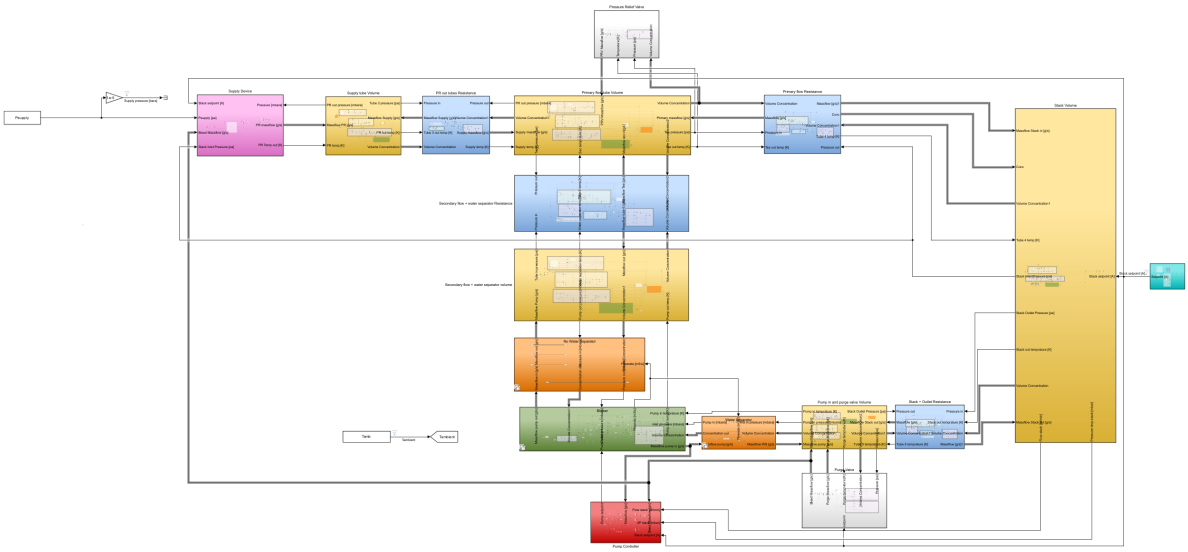

Figure B.1: Matlab Simulink model

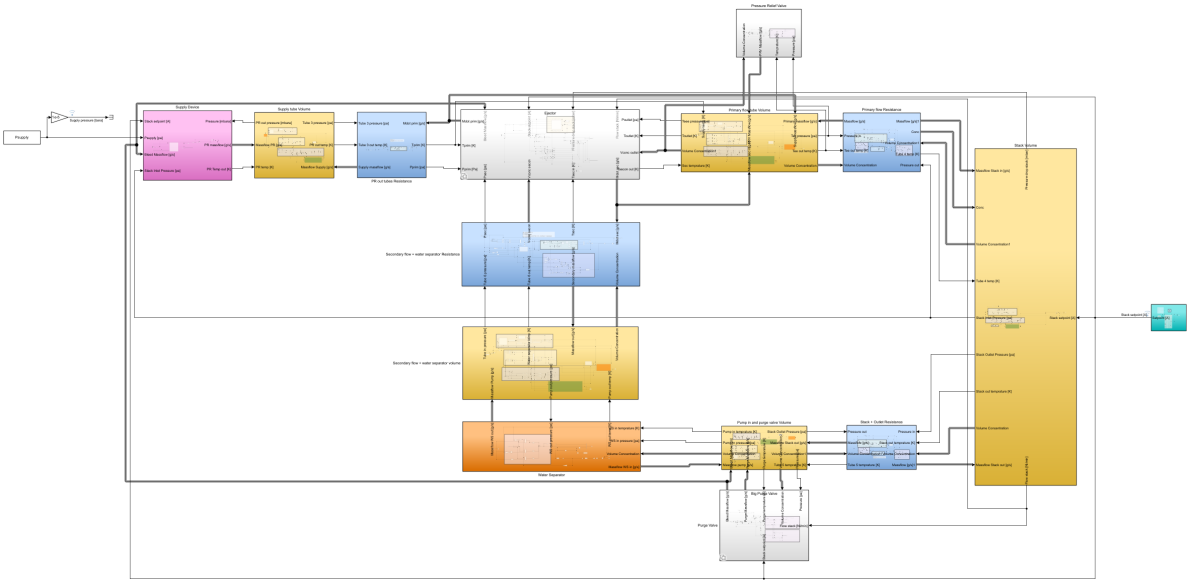

Figure B.2: Matlab Simulink model for the configurations with ejector

C

Equations

This appendix provides a detailed overview of the physical and empirical equations used in the dynamic model developed for simulating various hydrogen loop configurations. These equations form the foundation of the system behavior described in chapter 3, capturing the interactions between pressure, flow, temperature, humidity, and phase changes across the various components.

Unless stated otherwise, all equations are taken from [41]. The purpose of this appendix is to ensure transparency and reproducibility of the modeling methodology, allowing for validation of the simulation results and facilitating future modifications or extensions to the model.

C.1. Flow

Flow between volumes is calculated based on the pressure difference between volumes and the resistance between them. The Darcy-Weisbach equation is commonly used to calculate pressure drop based on flow conditions, see equation C.1 where Δp is the pressure drop, ρ is the fluid density, f is the friction factor, L is the pipe length, D is the diameter, and v is the fluid velocity. To account for minor losses due to bends, diameter changes, and fittings, an equivalent additional length was estimated based on the 3D model provided by Future Proof Shipping. This was added to the physical tube length to obtain the effective length used in the calculations.

$$\Delta p = \frac{1}{2}\rho f \frac{L}{D} v^2 \tag{C.1}$$

Since pressure drop is used as an input, the velocity must be derived accordingly. And can be rewritten as equation C.2.

$$v = \sqrt{\frac{2\Delta p}{\rho f \frac{L}{D}}} \tag{C.2}$$

The friction factor can be calculated with the use of the Reynolds number, which is used to determine the flow regime, see equation C.3, where μ is dynamic viscosity. When laminar, the friction factor is calculated with equation C.4 and when turbulent, with the Haaland-equation, see equation C.5, where ε is the pipe roughness. For Reynolds numbers between 2300 and 4000, a weighted average of both friction factors is taken.

$$Re = \frac{\rho v D}{\mu} \tag{C.3}$$

$$f = \frac{64}{Re}, Re < 2300 \tag{C.4}$$

$$f = \frac{1}{\left[-1.8log(\frac{\varepsilon/D}{3.7} + \frac{6.9}{Re})\right]^2}, Re > 4000 \tag{C.5}$$

Under laminar conditions, the velocity can be calculated directly using equations C.1, C.3, and C.4, which simplifies to equation C.6. In turbulent regimes, however, the friction factor depends on the velocity itself, requiring an iterative solution. To avoid algebraic loops in Simulink, a transfer function is used to approximate the friction factor based on the velocity from the previous time step.

$$v = \frac{\Delta p D^2}{32 \mu L}, Re < 2300 \tag{C.6}$$

As the gas flow is not pure hydrogen and also consists of water vapour, the density and the viscosity of the mixture need to be calculated based on their concentration. For density, this is done with equation C.7, where x_{H2} and x_{Vapour} are molar fractions, M_{H2} and M_{H2O} are molar masses, p is pressure, R is the gas constant, and T is temperature.

$$\rho_{mix} = \frac{(x_{H2} M_{H2} + x_{Vapour} M_{H2O}) p}{RT} \tag{C.7}$$

For calculating the dynamic viscosity, Wilke's method is used, see equation C.8, where ϕ_{ij} is the interaction parameter and is calculated with equation C.9.

$$\mu_{mix} = \sum_i x_i \mu_i \frac{\sum_j x_j \phi_{ij}}{\sum_j x_j} \tag{C.8}$$

$$\phi_{ij} = \frac{\left[1 + \left(\frac{\mu_j}{\mu_i}\right)^{0.5} \left(\frac{M_i}{M_j}\right)^{0.25}\right]^2}{\sqrt{8(1 + M_j/M_i)}} \tag{C.9}$$

Besides water vapour, there is also liquid water in the stream, so two-phase pressure drop calculations are needed, this is done with the Lockhart-Martinelli parameter χ. This parameter is calculated with equation C.10 [42].

$$\chi = \sqrt{\frac{\Delta p_{liquid}}{\Delta p_{gas}}} \tag{C.10}$$

When both phases are laminar, it can be simplified to equation C.11 and is no longer a function of velocity, where the C terms represent volume concentrations.

$$\chi = \sqrt{\frac{\mu_{liquid} C_{liquid}}{\mu_{mixture}(C_{H_2} + C_{vapour})}}, Re < 2300 \text{ both phases} \tag{C.11}$$

When the gas flow becomes turbulent, it can be simplified to C.12, however the friction factor is dependent on velocity, so this method requires the use of a transfer function to prevent an algebraic loop.

$$\chi = \sqrt{\frac{f_{liquid} \rho_{liquid}}{f_{gas} \rho_{mixture}}}, Re < 2300 \text{ liquid phase}, Re > 2300 \text{ gas phase} \tag{C.12}$$

The Lockhart-Martinelli parameter can then be used in equation C.13 to get a two-phase multiplier [43]. The C is the Chisholm Constant and is dependent on the flow regimes of both phases, it is 5 when both phases are laminar and 12 when the gas phase is turbulent and the liquid phase is laminar. None of the other options occur in this simulation. Lastly, equation C.14 can be used to convert the pressure drop of the gas phase to the two-phase pressure drop.

$$\Phi_g^2 = 1 + C\chi + \chi^2 \tag{C.13}$$

$$\Delta p_{twophase} = \Phi_g^2 \Delta p_{gas} \tag{C.14}$$

The speed of the fluid stream can then be converted to a volume flow $\dot{V}$, with the use of equation C.15. Together with the volumetric concentration, the mass flow of the hydrogen, vapour, and liquid stream can be calculated with equation C.16.

$$\dot{V} = v\pi(\frac{D}{2})^2 \tag{C.15}$$

$$\dot{m}_i = \dot{V}\rho_i C_i \tag{C.16}$$

Due to the large number of cells within a fuel cell stack, the flow velocity in each fuel cell channel is relatively low. Additionally, the small channels in the fuel cell contribute to a low Reynolds number. When the Reynolds number falls below 2300, laminar flow can be assumed, implying that the pressure drop is directly proportional to the flow velocity. Nedstack has supplied the pressure drop data for nominal operating conditions, enabling the calculation of pressure drop across all operating points.

Modeling pressure drop is critical for comparing various configurations and understanding their impact. So further research has been done on the effect of certain parameters on the pressure drop. A comparison of the effect of nitrogen, temperature, and water on pressure drop can be found in appendix D.

C.2. Temperature

The temperature is calculated in each volume at two places, the wall and the fluid stream. The fluid stream temperature is influenced by the incoming and outgoing fluid stream and heat transfer with the wall. For the wall, there is heat transfer with the fluid stream and the ambient air. All heat flows are integrated over time to calculate the accumulated heat in both the gas fluid stream and the surrounding wall. Using the resulting values, the temperature of the fluid stream and the wall is determined using equation C.17. This temperature is then used as the outlet temperature of the volume. In equation C.17, Q represents the accumulated heat, Cp is the specific heat capacity, and m is the mass of the medium.

$$T = \frac{Q}{\sum_i Cp_i m_i} \tag{C.17}$$

The heat of the incoming and leaving fluid stream is calculated with equation C.18, where $\dot{m}$ is the mass flow, the assumption is made that all 3 species have the same bulk temperature.

$$\dot{Q}_{stream} = Cp_i \dot{m}_i T \tag{C.18}$$

Heat transfer from the wall to the ambient is calculated with equation C.19. The thermal resistance due to conduction through the tube is calculated with equation C.20, where t is wall thickness, K is thermal conductivity and A the surface area.

$$\dot{Q}_{external} = \frac{\Delta T}{R_{wall} + R_{external}} \tag{C.19}$$

$$R_{wall} = \frac{t}{KA} \tag{C.20}$$

Free convection with the ambient air is calculated with equation C.21, where h is the heat transfer coefficient.

$$R_{external} = \frac{1}{hA} \tag{C.21}$$

The external heat transfer coefficient is then calculated with equation C.22. The Nusselt number, which is calculated with equation C.23, this equation can be used as the Rayleigh number is below 10^9. Dimensionless numbers Ra, Pr, and Gr are calculated with equations C.24, C.25, C.26, where β is the coefficient of volume expansion, g is the gravitational constant and ν is the kinematic viscosity.

$$h = \frac{kNu}{D} \tag{C.22}$$

$$Nu = 0.36 + \frac{0.518Ra^{1/4}}{\left(1 + (0.559/Pr)^{9/16}\right)^{4/9}} \tag{C.23}$$

$$Ra = GrPr \tag{C.24}$$

$$Pr = Cp\frac{\mu}{k} \tag{C.25}$$

$$Gr = \frac{\beta \Delta T g D^3}{\nu^2} \tag{C.26}$$

For the heat transfer between the tube walls and the fluid stream equation C.27 is used, where U is the heat transfer coefficient. The heat transfer coefficient is calculated with equation C.28. The Nusselt number for internal heat transfer is calculated with equation C.29 or equation C.30 when the Reynolds number is low. The friction factor is calculated with equation C.5 and the Prandtl number with equation C.25.

$$\dot{Q}_{internal} = U\Delta T A_{surfacearea} \tag{C.27}$$

$$U = k\frac{Nu}{D} \tag{C.28}$$

$$Nu = \frac{\frac{f}{8}(Re - 1000)Pr}{1 + 12.7\frac{f}{8}^{1/2}(Pr^{2/3} - 1)}, Re > 3000 \tag{C.29}$$

$$Nu = 3.66, Re < 3000 \tag{C.30}$$

Heat flow for condensation is calculated with equation C.31, where $H(T)$ is the latent heat of evaporation is dependent on temperature, for this, a simple approximation is made with a formula. The heat is then split between the wall and fluid stream according to equation C.32, U is taken from equation C.28, R_{wall} is taken from equation C.20.

$$\dot{Q}_{cond} = H(T)\dot{m}_{cond} \tag{C.31}$$

$$\text{Fraction of heat to the wall} = \frac{\frac{1}{R_{wall}}}{\frac{1}{R_{wall}} + \frac{1}{R_{internal}}} \tag{C.32}$$

$$R_{internal} = \frac{1}{AU} \tag{C.33}$$

C.3. Evaporation and condensation

Through the system, phase change will happen to the water, so the condensation rate should be calculated, a negative condensation rate means evaporation is happening. This can be calculated with equation C.34, $\Delta\rho$ is the concentration difference between the fully saturated and the current concentration. This concentration difference is calculated with equations C.35 and C.36. Condensation can only occur when there is vapour, and evaporation can also only occur when there is liquid present.

$$\dot{m}_{condensation} = \Delta\rho h_m A_{surfacearea} \tag{C.34}$$

$$\Delta\rho = \frac{\Delta p M_{H2O}}{RT} \tag{C.35}$$

$$\Delta p = RH * P_{sat} - P_{sat} \tag{C.36}$$

The mass transfer coefficient is calculated with the Sherwood number, according to equation C.37, where D_v is the diffusion coefficient.

$$h_m = \frac{ShD_v}{D} \tag{C.37}$$

The Sherwood number is based on the flow regime, when laminar with equation C.38, with a minimum of $Sh > 3.66$.

$$Sh = 1.86\left(ReSc\frac{D}{L}\right)^{\frac{1}{3}}, Re < 2300 \tag{C.38}$$

When turbulent equation C.39 should be used, this equation uses the Schmidt number, which is calculated with equation C.40. All the equations in this section come from [44].

$$Sh = 0.023Re^{\frac{4}{5}}Sc^{\frac{2}{5}}, Re > 2300 \tag{C.39}$$

$$Sc = \frac{\mu}{\rho D_v} \tag{C.40}$$

D

Pressure drop

The following sections analyze the dynamic factors contributing to increased pressure drop. For all cases, the pipe and flow parameters are the same. For this section, the relative values of these calculations are more important than their absolute values.

D.1. Effect of water on pressure drop

As seen in section 2.6, the water crossover can be quite high (up to 30%). This means that at the maximum setpoint, 40 g/s of water will be produced, of which 12 g/s could crossover to the anode side. This water will be partly in vapour form and partially liquid, depending on temperature. This will mean that the stream will be in two-phase flow. This adds complexity to the pressure drop calculations. Figure D.1 shows the pressure drop for an increasing amount of water, due to higher water crossover. One can clearly see the transition when the stream saturates.

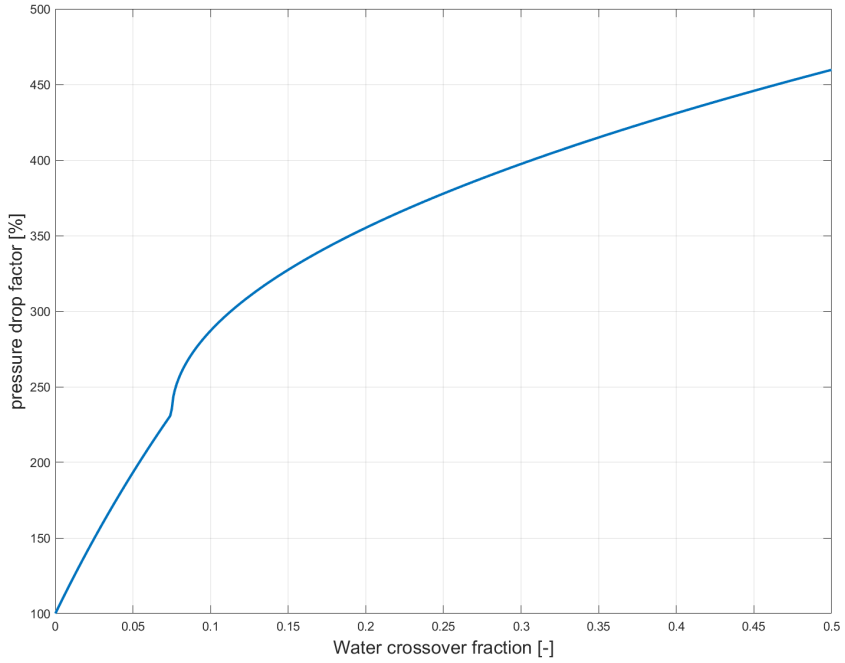

Figure D.1: Pressure drop factor with increasing water crossover

D.2. Effect of nitrogen on pressure drop

In section 2.6 the cause of water and nitrogen crossover was discussed, here the effect it has on pressure drop will be addressed. Due to the addition of nitrogen into the hydrogen stream, two properties

change that affect the pressure drop. The first is the density of the mixture, this can be simply calculated by taking the density of both gases and their molar concentration, as equation C.7 shows. Secondly, the viscosity changes which is less straightforward to calculate. Values from experiments were taken and interpolated [45]. In figure D.2a, one can see the viscosity of the mixture based on the molar concentration of nitrogen at 50 °C.

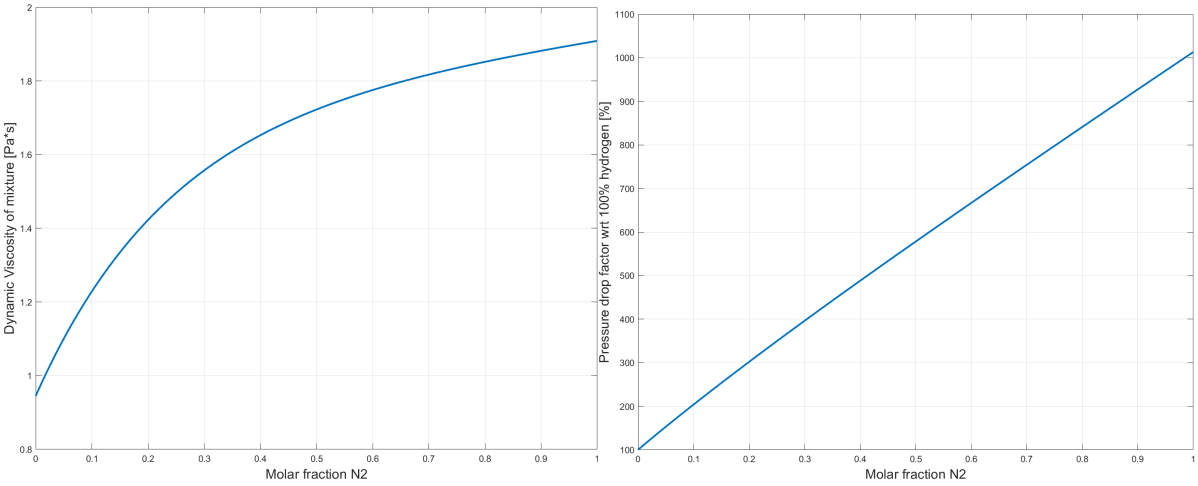

(a) Dynamic viscosity of a hydrogen and nitrogen mixture

(b) Pressure drop factor compared to pure hydrogen

Figure D.2: Effects of nitrogen on pressure drop

In figure D.2b, one can see how much the pressure drop increases with increasing nitrogen concentration. A drop from 100% to 90% hydrogen concentration will result in roughly double the pressure drop and thus also double the power required by the pump.

D.3. Effect of temperature on pressure drop

The influence of temperature on pressure drop is shown in figure D.3. Compared to the previously discussed factors, temperature has a minimal effect on pressure drop.

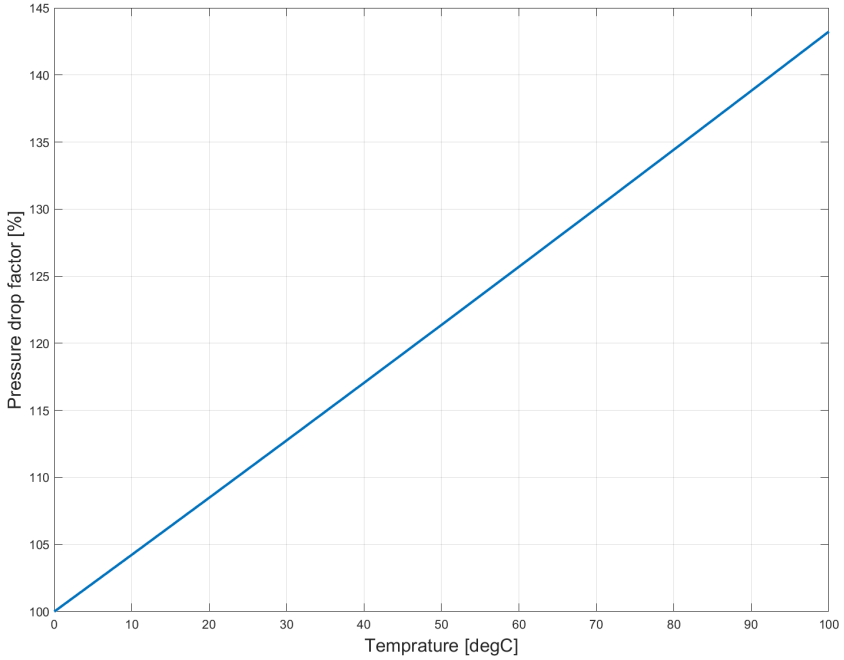

Figure D.3: Pressure drop factor with increasing temperature

The findings indicate that accurate modeling of water content is crucial for understanding pressure drop and maintaining fuel cell efficiency. Since water and humidity are highly temperature dependent, proper temperature modeling is essential. Although nitrogen has a substantial effect on pressure drop, the limited amount of nitrogen crossover minimizes its overall impact, allowing it to be ignored in this context.

E

Validation

Table E.1 shows a comparison of the data from the ship and the simulation. Parameters were adjusted to align with both datasets. The biggest deviation can be seen with the temperature readings, the best explanation for this is that the sensor placement on the ship is different from where the model measures them.

Table E.1: Comparison of ship's data and simulation data at two setpoints

	Setpoint	PR out	Stack in	Stack in	Purge duty	Stack out	Stack out	Secondary	Pump setpoint		dP stack	dT pump
	[kW]	[°C]	[mbar]	[°C]	[%]	[mbar]	[°C]	[°C]	[%]		[mbar]	[°C]
Ship data	301.83	14.2	273.9	49.1	90	231.91	57.1	63	100		42.0	5.9
Simulation data	300	14.2	280.85	46.9	90	235.55	59.9	65.9	100		45.3	6.0
Deviation		0	6.95	-2.2	0	3.64	2.8	2.9	0		3.3	0.1
Ship data	200.8	15.29	298.7	53.86	79.41	258.05	56.95	63.22	100		40.7	6.3
Simulation data	200	15.3	292.4	52.0	79.4	253.9	60	66	100		38.5	6
Deviation		0.01	-6.3	-1.9	0.0	-4.2	3.05	2.78	0		-2.1	-0.3

F

Scores

Figure F.1 shows what score each performance indicator gets for a certain value. For scores within what the stack manufacturer specifies, the score is 100. Outside this range, the score drops, as can be seen in the figure. Depending on how critical this parameter is, the score drops sharper. How these scores are determined can be seen in section 3.5.

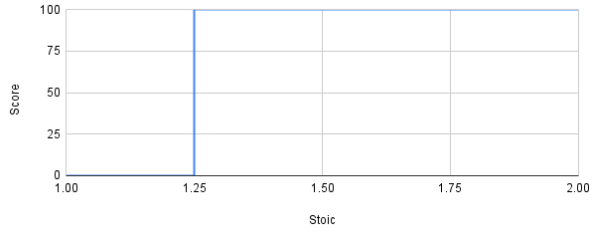

(a) Stoichiometry score

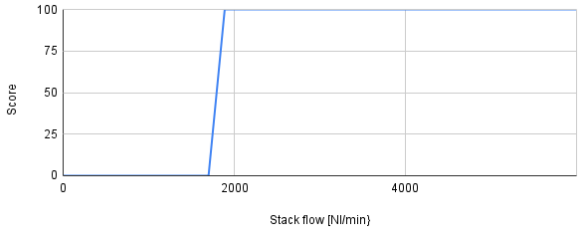

(b) Minimum flow stack score

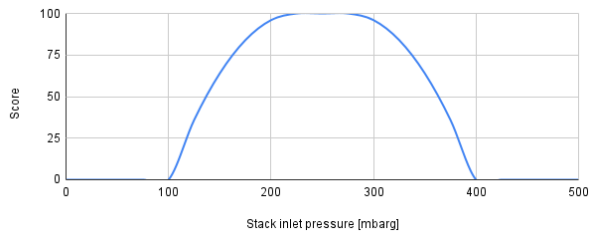

(c) Pressure score

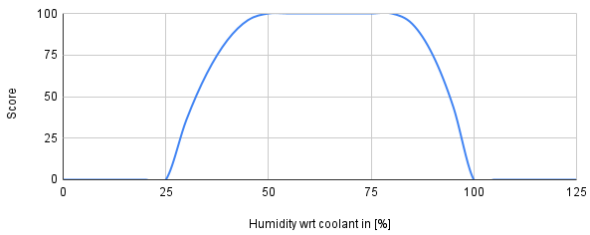

(d) Relative humidity score

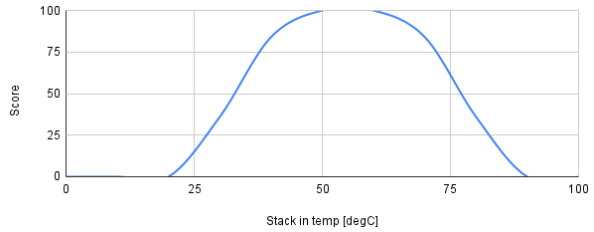

(e) Temperature score

Figure F.1: Scoring of each key performance indicator

G

Pressure robustness

To evaluate the pressure robustness of each configuration, three simulations were conducted at different supply pressures: 8, 10, and 12 bar. The load profile used in these tests is identical to the one shown in figure 4.1. Some configurations produced identical pressure responses across the tested pressures; for clarity and improved readability, only one representative plot is shown for those cases in figure G.1.

Figure G.1 is organized into three rows. The top row presents the raw pressure traces over time. The middle row shows the same data, filtered to exclude pressure values above 450 mbar, as those points would trigger the pressure relief valve and would skew the results. The bottom row displays the pressure fluctuations after filtering. The final quantitative results derived from these plots are summarized in table 4.5.

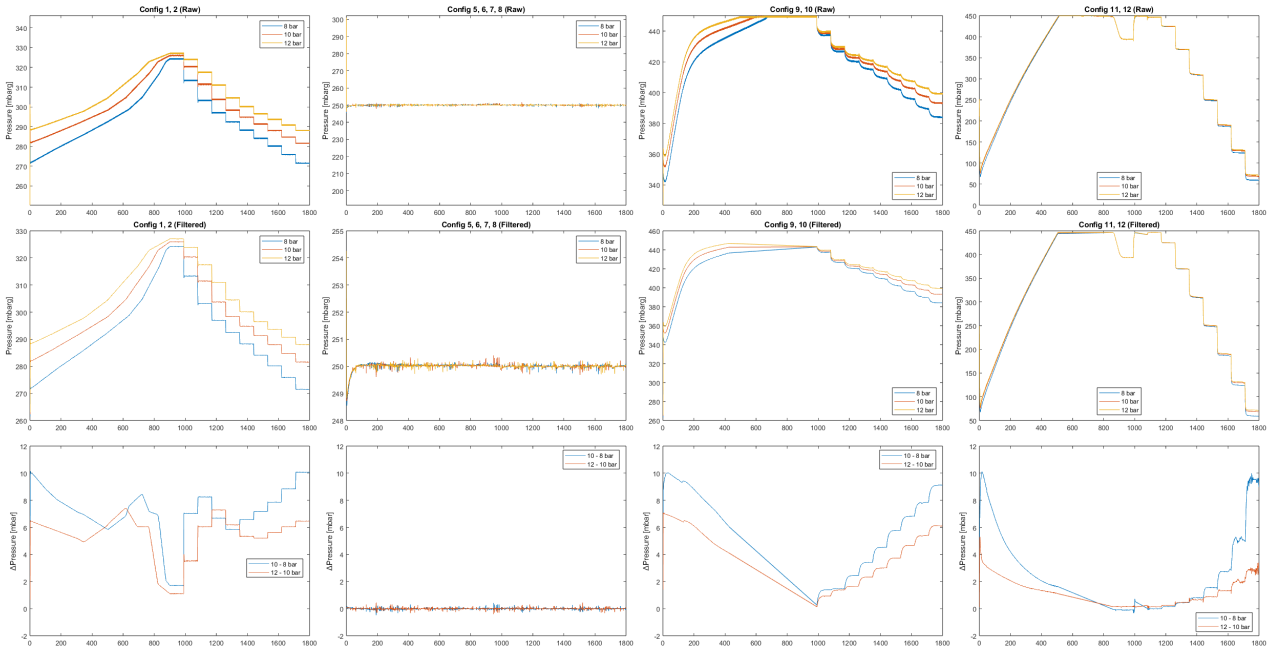

Figure G.1: Pressure profiles for various configurations under different supply pressures.

H

Transient behavior Results

Figure H.1 shows the transient response of pressure and stoichiometry during step changes in load, specifically from 10% to 100% and vice versa. Only the 10% to 100% transitions are shown here, as they represent the most significant change and therefore highlight differences in system behavior more clearly. The dashed lines indicate system responses without a rate limiter applied. Configurations 3

and 4 are not included in this analysis, as their limited operating range prevents them from completing the full load transition. Most configurations respond well to the step change, with smooth transitions in both pressure and stoichiometry. In some cases, the absence of a rate limiter results in brief spikes, but these are generally not problematic, especially considering that omitting a rate limiter is not a realistic operating scenario. Overall, it is difficult to draw strong conclusions from these plots alone, as differ-

ences between configurations are relatively minor. However, the results suggest that the hydrogen loop is unlikely to be the limiting factor in the BoP when it comes to transient performance.

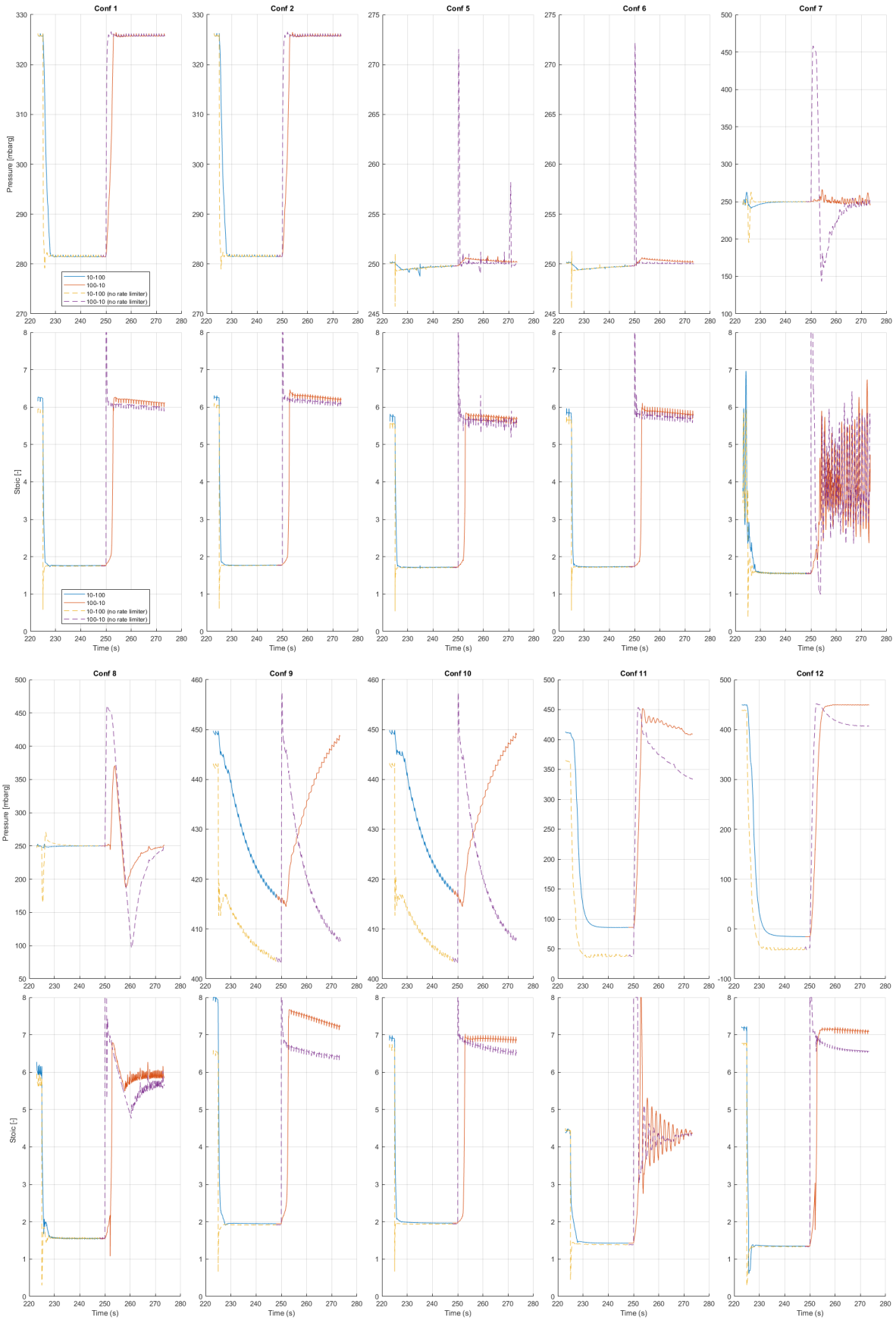

Figure H.1: Pressure and stoichiometry response to load step changes (10% to 100%) with/without rate limiter

Parameters dependence

Figure I.1 presents box plots showing the distribution of scores for each key parameter, grouped by device type. Each box plot includes all relevant scores associated with that device across different configurations, highlighting how device selection influences system performance.

From the pressure plot, it is evident that the supply device predominantly determines pressure behavior. In contrast, both relative humidity and temperature are strongly influenced by the recirculation device, as these parameters are closely tied to the amount and characteristics of recirculated flow.

Efficiency scores for the ejector exhibit the widest spread, ranging from the highest to the lowest values among all devices. This variation is primarily due to the additional purging required at low loads, which significantly impacts hydrogen utilization. Lastly, the minimum flow requirement through the stack was consistently met by all pump types.

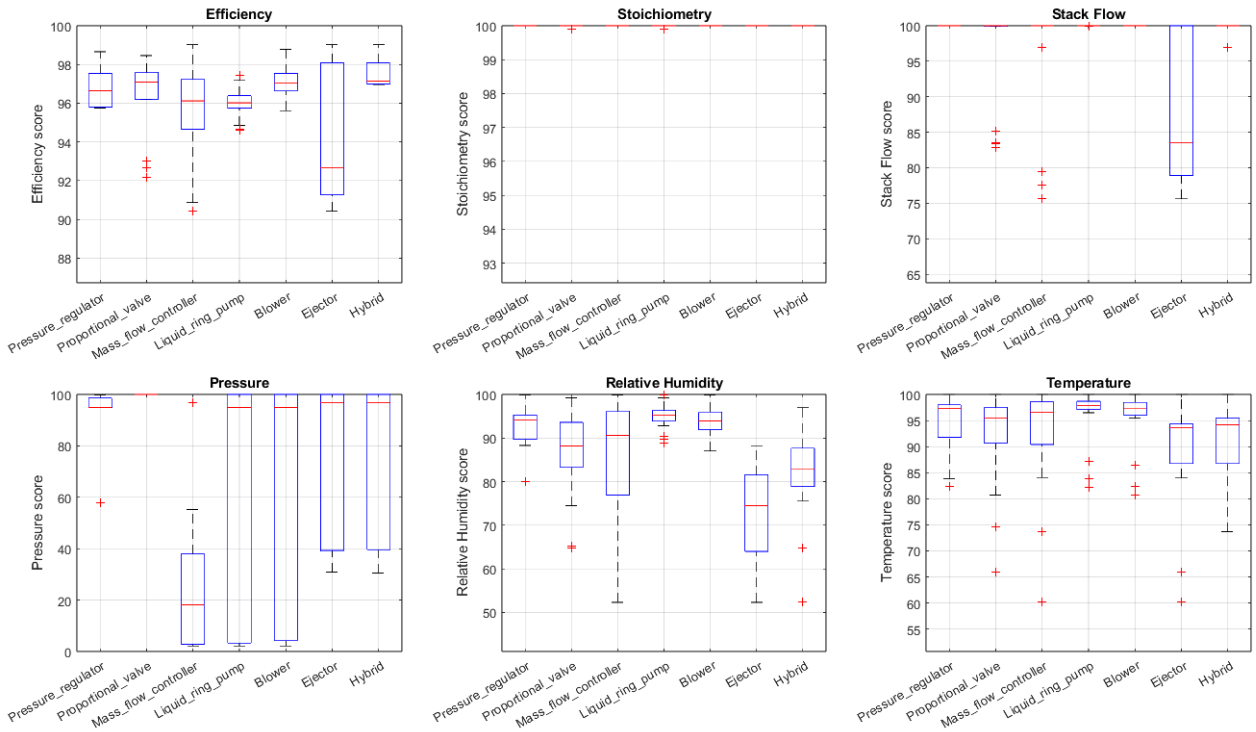

Figure I.1: Box plots for each key parameter and device